

Impact of Higher-Order Modes on Eccentricity Measurement in Binary Black Hole Gravitational Waves

Honglue Tang¹, Jinzhao Yang¹, Baoxiang Wang¹, and Tao Yang^{1,*}

¹*School of Physics and Technology, Wuhan University, Wuhan 430072, China*

(Dated: February 5, 2026)

We investigate the systematic biases in measuring orbital eccentricity for binary black hole (BBH) mergers that arise when higher-order modes (HOMs) of gravitational waves are neglected in waveform modeling. Using Bayesian inference with the state-of-the-art eccentric, spin-aligned, higher-mode effective-one-body model SEOBNRv5EHM, we reanalyze six previously suggested eccentric gravitational-wave events—GW190521, GW190620, GW190701, GW191109, GW200129, and GW200208_222617. Comparing results with its dominant-mode-only counterpart SEOBNRv5E, we find no statistically significant HOM-induced bias in eccentricity for any of these events, including GW190521, whose eccentricity has been debated in the literature. To identify parameter regimes vulnerable to HOM omission, we perform a broad zero-noise injection campaign varying detector-frame total mass, mass ratio, eccentricity, inclination, and network SNR. We find that significant systematic biases ($\Delta_e/\sigma > 1$) arise predominantly in systems with high total mass ($M^{\text{det}} \gtrsim 120M_{\odot}$), highly asymmetric mass ratios ($q \gtrsim 4$), near edge-on orientations ($\theta_{\text{JN}} \gtrsim 30^\circ$), and high SNRs ($\rho_{\text{mf}}^N \approx 50$). Notably, for quasi-circular BBHs with $M^{\text{det}} \gtrsim 140M_{\odot}$, neglecting HOMs may lead to strong false-positive evidence for nonzero eccentricity. By contrast, for lower-mass systems ($M^{\text{det}} \sim 100M_{\odot}$), HOM exclusion produces negligible eccentricity biases. Our results demonstrate that although current eccentric candidates are not impacted by HOM omission, future eccentricity measurements—particularly for massive, asymmetric, or edge-on systems—require HOM-inclusive waveforms to avoid substantial systematic errors.

I. INTRODUCTION

Since the first detection of gravitational waves (GWs) in 2015 [1], the LIGO-Virgo-KAGRA (LVK) Collaboration [2–4] has released four Gravitational-Wave Transient Catalogs (GWTC), reporting more than 200 GW events up to the first part of the fourth observing run (O4a) [5–8]. These observations have enabled many applications in cosmology, astrophysics and fundamental physics, such as the constraint of cosmic expansion [9–13], population studies of compact binaries [14–17], and test of general relativity (GR) and black hole physics [18–26]. Most GW events observed to date are attributed to the compact binary coalescences (CBCs), including binary black holes (BBHs), binary neutron stars (BNSs) and neutron star-black hole (NSBH) systems. However, their astrophysical formation channels remain uncertain.

There are two leading formation channels proposed for CBCs: isolated evolution and dynamical formation [16, 27–35]. In isolated evolution, two stars evolve together, form black holes, and finally coalesce with GW emission [31–33, 36–39]. Over long evolution timescales, the orbital eccentricity of binaries efficiently dissipates with GW emissions, leading to nearly circularized orbits by the time the GW frequency f enters the observing band of ground-based GW detectors like LIGO (e.g., $f \gtrsim 10$ Hz) [40]. Dynamical formation refers to coalescences formed via dynamical interactions [41–43], including dynamical capture [44–46] and multi-body en-

counters [47–49], which usually occur in dense environments such as active galactic nuclei (AGN) and globular clusters [50–52], as dynamical interactions happen more frequently in such environments. Unlike isolated evolution, binaries formed dynamically can retain measurable orbital eccentricity in the observing band due to the short duration from encounter to merger [53–55] or external disturbance such as the Kozai-Lidov oscillations [56–61]. Therefore, orbital eccentricity provides a useful tool to distinguish astrophysical formation channels [62]. Beyond its importance in astrophysics, some studies have pointed out that eccentricity can greatly improve the parameter estimation (PE) and localization of GW sources [63–68]. Moreover, Yang et al. proposed that eccentricity-induced higher harmonics can significantly enhance early warning of the detection and localization of GWs [69, 70]. On the other hand, ignoring eccentricity can induce systematic biases in PE and loss in signal recovery, affecting the GW application in astrophysics and test of GR [71–77]. Therefore, the measurement of orbital eccentricity and relevant data analysis have become an essential aspect in GW astronomy.

The LVK collaboration has not confirmed any eccentric event with waveform-independent analysis [78, 79]. Nevertheless, some research groups have independently reported several eccentric candidates based on waveform-dependent methods. Applying the eccentric waveform model SEOBNR with likelihood reweighting, Romero-Shaw *et al.* [80, 81] identified GW190521 and GW190620 as eccentric candidates. They later reported two additional candidates, GW191109 and GW200208_222617, with the same approach [82]. In parallel, Gayathri *et al.* [83] reported $e \approx 0.69$ for GW190521 through

* Corresponding author: yangtao@whu.edu.cn

a numerical-relativity (NR) method. Furthermore, a machine-learning-based analysis using SEOBNRv4EHM reported three potential eccentric events: GW190701, GW200129, and GW200208_222617 [84]. The most recent analysis with the phenomenological, eccentric model IMRPhenomTEHM reanalyzed 17 events, reporting strong support for eccentricity in GW200129 and GW200208_222617, with weaker evidence in GW190701 and GW190929 [85].

Among these eccentric candidates, GW190521 has some notable source properties. It was the most massive BBH observed at the time, with a total mass of $153 M_{\odot}$ in the source frame [86]. The remnant black hole provides the first clear evidence for an intermediate-mass black hole, while the primary black hole is highly likely to lie within the pair-instability mass gap, suggesting a possible hierarchical merger. Moreover, Graham *et al.* [87] reported a potential electromagnetic counterpart of GW190521 consistent with a kicked BBH merger in an AGN disk. All of the features mentioned above support the idea that GW190521 could have formed in a dynamical scenario, which in turn may suggest a non-zero eccentricity. Intriguingly, early analyses using SEOBNRE and NR support that GW190521 is eccentric [80, 83]. However, using later developed waveforms including higher-order modes (HOMs), which are the multipolar components of GWs beyond the dominant $(\ell, |m|) = (2, 2)$ mode, subsequent studies found no sign of eccentricity in GW190521 [84, 88–90]. This is a well-known tension of the measurement of eccentricity in current GW catalogs. This tension could result from the incompleteness of waveform models, differences in analysis methods, or other unknown effects. Some studies have shown that omitting HOMs in waveforms may lead to significant systematic biases in parameter estimation [91–93]. We note that this tension originates from the conflicting results between Ref. [80] and Refs. [84, 88–90]. The former used (2,2)-mode-only waveform SEOBNRE, while the latter employed HOM-included waveform models, such as SEOBNRv4EHM, TEOBResumSGeneral, and SEOBNRv5EHM. This motivates us to investigate whether neglecting HOMs in waveform models could account for this tension.

Eccentric waveform modeling has advanced considerably from early post-Newtonian (PN) inspiral-only templates [94–104] to current inspiral-merger-ringdown (IMR) models which are calibrated with NR [105–119]. A general approach for many recent eccentric IMR models employs the effective-one-body (EOB) formalism, which combines PN dynamics with NR calibration to construct semi-analytical waveform models. Representative waveform families include SEOBNR and TEOBResumS. Early EOB models were based on the spin-aligned assumption, with spin precession and HOMs omitted. (e.g., SEOBNRE [113, 114]). More current EOB eccentric models incorporate aligned (or misaligned) spins and HOMs (e.g., SEOBNRv5EHM [90], and TEOBResumSDali [118]), with some models developed from SEO-

NRE further including spin precession [120]. In parallel, a phenomenological, spin-aligned, HOM-included, eccentric IMR model, IMRPhenomTEHM, has recently been proposed, providing an efficient alternative for eccentric GW studies [119]. For the computational efficiency and model accuracy, in this work, we employ the state-of-the-art eccentric waveform SEOBNRv5EHM [90] to analyze the systematic biases in the measurement of orbital eccentricity due to omitting HOMs in the GW waveforms.

In this work, we first investigate whether the tension in the measurement of GW190521's eccentricity is caused by omitting the HOMs in the waveforms. To do this, we employ SEOBNRv5EHM and the dominant-only modes of SEOBNRv5EHM $(\ell, |m|) = (2, 2)$, henceforth referred to as SEOBNRv5E) to reanalyze GW190521 and compare the constraints of eccentricity with the two models. Beyond GW190521, we also reanalyze the other five eccentric candidates and assess whether their eccentricity measurements are affected by the HOMs. Moreover, we intend to identify the regions of parameter space (e.g., total masses, mass ratios, inclination angles, etc.) where neglecting HOMs could introduce significant systematic biases in eccentricity measurements. To investigate this, we carry out a systematic injection-recovery study by sampling over five parameters: the total mass $M = m_1 + m_2$, mass ratio $q = m_1/m_2 \geq 1$, orbital eccentricity e , inclination angle θ_{JN} , and matched-filter network SNR ρ_{mf}^N . The injections are based on the LIGO and Virgo detector network for consistency with GW detections, and the injected luminosity distance is adjusted to achieve the desired network SNR. For each injection, we generate HOM-included waveforms employing SEOBNRv5EHM and recover parameters using SEOBNRv5E.

This paper is organized as follows. Sec. II describes our methodology. The analysis of eccentric GW candidates is presented in Sec. III, followed by injection studies in Sec. IV. In Sec. V, we conclude the results with further discussions.

II. METHODOLOGY

A. Eccentric Waveform Models

We employ the time-domain EOB waveform model SEOBNRv5EHM implemented in the `pySEOBNR` package, which is designed for spin-aligned BBHs incorporating eccentricity and higher-order modes [90, 121]. For parameter estimation, time-domain waveforms are converted to the frequency domain via the Fourier transform. As a member of the state-of-the-art SEOBNR family, SEOBNRv5EHM targets eccentric BBHs with moderate eccentricity and has been validated up to $e \approx 0.5$ at $f = 20$ Hz, being among the most accurate eccentric waveform models available at the time of publication.

SEOBNRv5EHM describes eccentric binaries using a

Keplerian parameterization of the eccentric orbit:

$$r = \frac{M}{u_p(1 + e \cos \zeta)}, \quad (1)$$

where $M = m_1 + m_2$ represents the total mass in geometric units with m_1, m_2 being the component masses, e corresponds to the Keplerian orbital eccentricity, ζ represents the relativistic anomaly, and u_p is the inverse semilatus rectum. All parameters are specified at the user-defined starting frequency f_0 , which corresponds to the dimensionless orbit-averaged orbital frequency $\langle M\Omega \rangle$, and Ω represents the instantaneous orbital frequency. For simplicity, all eccentricities and relative anomaly discussed hereafter are defined at the starting frequency, denoted as e_0 and ζ_0 .

SEOBNRv5EHM contains the dominant $(\ell, |m|) = (2,2)$ mode and HOMs $(\ell, |m|) = (2,1), (3,3), (3,2), (4,4), (4,3)$. It constructs the gravitational polarizations according to this equation:

$$h_+ - i h_\times = \sum_{l=2}^{\infty} \sum_{m=-l}^l -_2 Y_{\ell m}(\theta_{\text{JN}}, \varphi) h_{\ell m}(\Theta, t), \quad (2)$$

where $-_2 Y_{\ell m}$ are the spherical harmonics of -2 spin-weight depending on the inclination angle θ_{JN} and azimuthal angle φ , $h_{\ell m}$ are the gravitational-wave modes, and Θ represents the binary's intrinsic parameters. These modes include 3PN eccentricity corrections to the EOB radiation reaction force and the inspiral phase, while the merger-ringdown phase is modeled based on a quasi-circular assumption. In the zero-eccentricity limit, SEOBNRv5EHM is demonstrated to be consistent with SEOBNRv5HM [122]. Comparing against NR eccentric waveforms from the Simulating eXtreme Spacetimes Collaboration, the $(2,2)$ mode of SEOBNRv5EHM achieves a median unfaithfulness of $\sim 0.02\%$ with a total mass range of $20 - 200 M_\odot$ and eccentricity up to 0.5 at $f = 20$ Hz [90]. Compared with its predecessor, SEOBNRv4EHM [116], SEOBNRv5EHM improves in computational efficiency, model accuracy, and validated parameter space coverage. Under commonly used settings, SEOBNRv5EHM yields a slightly shorter PE runtime for GW150914 and GW190521 than SEOBNRv4EHM_opt, an optimized version of SEOBNRv4EHM [89, 90]. Based on our estimation, the improvement is approximately 2-5 times faster.

B. Bayesian Inference

Bayesian inference is a fundamental tool for data analysis and parameter estimation in GW astronomy [123, 124]. According to Bayes' theorem, the probability distribution of parameter θ given measured GW signal d and model \mathcal{H} is obtained by

$$p(\theta|d, \mathcal{H}) = \frac{\mathcal{L}(d|\theta, \mathcal{H})\pi(\theta|\mathcal{H})}{\mathcal{Z}}, \quad (3)$$

where $\pi(\theta|\mathcal{H})$ is the prior distribution of parameter θ given \mathcal{H} , $\mathcal{L}(d|\theta, \mathcal{H})$ is the likelihood function, and \mathcal{Z} is the evidence of model \mathcal{H} given measured data,

$$\mathcal{Z} = \int \mathcal{L}(d|\theta, \mathcal{H}) \pi(\theta|\mathcal{H}) d\theta. \quad (4)$$

We adopt a Gaussian likelihood function, assuming an N-detector network with zero-mean, stationary, Gaussian, and uncorrelated detector noise. The network log-likelihood is defined as the sum of single-detector Gaussian log-likelihoods,

$$\ln \mathcal{L}(d|\theta, \mathcal{H}) \propto -\frac{1}{2} \sum_{i=1}^N \langle d - \mathcal{H}(\theta) | d - \mathcal{H}(\theta) \rangle_i, \quad (5)$$

where i represents the i -th detector and N is the number of detectors. The noise-weighted inner product of two signals A and B is defined as

$$\langle A | B \rangle_i \equiv 4\Re \int_{f_{\min}}^{f_{\max}} df \frac{\tilde{A}_i(f) \tilde{B}_i^*(f)}{S_n^{(i)}(f)}, \quad (6)$$

where $S_n^{(i)}(f)$ is the one-sided noise power spectral density (PSD) of the i -th detector, \tilde{A} and \tilde{B} represent the frequency-domain signal after the Fourier transform.

Parameter estimation is performed with `bilby` [125] and the nested sampler `dynesty` [126], using the following sampler settings: `sample='acceptance-walk'`, `naccept=60`, and `nlive=1000`. The sampling frequency is set to $f_{\text{samp}} = 4096$ Hz. For GW event analysis, we set minimum frequency $f_{\min} = 20$ Hz ($f_{\min} = 11$ Hz for GW190521, following [86, 90]). Meanwhile, the maximum frequency f_{\max} is 512, 448, 448, 448, 896, and 1792 Hz for GW190521, GW190620, GW190701, GW191109, GW200129, and GW200208_222617, respectively. For injection studies, we adopt $f_{\min} = 20$ Hz and $f_{\max} = 2048$ Hz.

The data segments are 8 seconds in duration, with a 2-second post-merger duration, for all GW event analyses, except for GW190701 and GW191109, for which 4-second segments are used due to data quality issues. For injections, we adopt the same 8-second segments. When comparing HOM-included and HOM-excluded results for the same event or injection, we utilize identical sampler settings and analysis pipelines. Any unspecified sampler settings are set to the default values in `bilby`.

C. Systematic Bias

We quantify the impact of neglecting HOMs on eccentricity estimation primarily using the posterior-based systematic errors. Throughout this article, we use "systematic bias" to refer to the bias effect in PE caused by ignoring HOMs, and "systematic error" to describe the quantitative difference between the true values (or specified reference values) and predicted values.

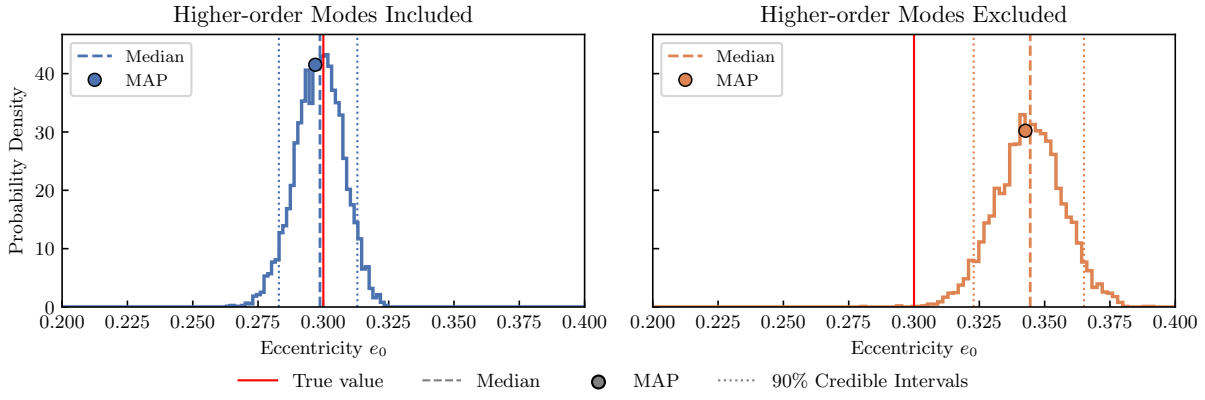


FIG. 1. The eccentricity posteriors for an example injected GW signal generated with SEOBNRv5EHM. The left panel shows the result recovered with SEOBNRv5EHM, while the right panel shows the result obtained with SEOBNRv5E. The red solid line indicates the true eccentricity. The colored dashed lines and circular markers show the median and MAP estimates of eccentricity, respectively. The colored dotted lines indicate the 90% credible interval of eccentricity posteriors. As shown in the figures, the exclusion of HOMs significantly biases the estimated orbital eccentricity. This GW signal is generated with $M = 160M_{\odot}$, $q = 6$, $e_0 = 0.3$, $\theta_{\text{JN}} = 90^\circ$, $\rho_{\text{mf}}^N = 50$, and $f_{\text{ref}} = 10$ Hz.

Let the observed data d be the combination of the true GW signal s and detector noise n ,

$$d = s + n. \quad (7)$$

Assume s can be explicitly described by a GW waveform model h_{tr} given a set of true parameters λ_{tr} (i.e., $s = h_{\text{tr}}(\lambda_{\text{tr}})$), and we use an approximate model $h_{\text{app}}(\lambda)$ to recover λ_{tr} , resulting in the joint parameter posteriors $p_{\text{app}}(\lambda)$ and estimated parameters λ_{app} . When the approximant model exactly matches the true signal, the maximum a posteriori (MAP) of $p_{\text{app}}(\lambda)$ is expected to satisfy $\lambda_{\text{app}}^{\text{MAP}} \approx \lambda_{\text{tr}}$ [72, 92]. In contrast, the model difference between h_{true} and h_{app} can lead to biases in the estimation of λ_{tr} . Fig. 1 presents an example using HOM-excluded models to recover the orbital eccentricity of an HOM-included signal. We define the systematic error Δ_{λ} between the estimated parameters λ_{app} and true parameters λ_{tr} to quantify such biases:

$$\Delta_{\lambda} = \lambda_{\text{app}} - \lambda_{\text{tr}}. \quad (8)$$

In our injection analysis, the injected signals are generated using the HOM-included waveform model SEOBNRv5EHM, so the true parameters λ_{tr} are equal to the injected parameters λ_{inj} (i.e., $\lambda_{\text{tr}} = \lambda_{\text{inj}}$). We employ the HOM-excluded SEOBNRv5E as the approximate model for parameter recovery, leading to $\lambda_{\text{app}} = \lambda_{22}$, where λ_{22} is the parameters estimated with SEOBNRv5E. We report both the median-based and MAP-based systematic error

$$\Delta_{\lambda}^{\text{Median}} = \lambda_{22}^{\text{Median}} - \lambda_{\text{inj}}, \quad \Delta_{\lambda}^{\text{MAP}} = \lambda_{22}^{\text{MAP}} - \lambda_{\text{inj}}. \quad (9)$$

λ^{MAP} is calculated as the MAP of the joint posterior and λ^{Median} is the median values of corresponding one-dimensional marginalized posteriors.

For GW events, the true value is actually unavailable. Therefore, we adopt SEOBNRv5EHM as an *approximately true* model, with its corresponding estimated parameters λ_{HM} as a fiducial reference (i.e., $\lambda_{\text{tr}} = \lambda_{\text{HM}}$). Similarly, we compare HOM-included results λ_{HM} and HOM-excluded results λ_{22} using both MAP-based and median-based errors:

$$\Delta_{\lambda}^{\text{Median}} = \lambda_{22}^{\text{Median}} - \lambda_{\text{HM}}^{\text{Median}}, \quad \Delta_{\lambda}^{\text{MAP}} = \lambda_{22}^{\text{MAP}} - \lambda_{\text{HM}}^{\text{MAP}}. \quad (10)$$

In our study, we primarily rely on the median-based errors, with the MAP-based errors provided as a supplementary approach.

To evaluate the significance of systematic biases, we report the normalized systematic error Δ_{λ}/σ , which is defined as the ratio of the systematic errors to their corresponding statistical errors σ_{λ} . Following [92], the statistical error σ_{λ} of the parameter λ is defined as

$$\sigma_{\lambda} = \begin{cases} Q_{100\%}(\lambda) - Q_{10\%}(\lambda), & \lambda_{\text{app}} > Q_{95\%}(\lambda) \\ Q_{90\%}(\lambda) - Q_{0\%}(\lambda), & \lambda_{\text{app}} < Q_{5\%}(\lambda) \\ [Q_{95\%}(\lambda) - Q_{5\%}(\lambda)]/2, & \text{else} \end{cases}, \quad (11)$$

where $Q_{N\%}(\lambda)$ represents the $N\%$ percentile of λ given its marginalized posterior $p(\lambda)$. Accordingly, the normalized systematic error of a specific parameter λ (i.e., e_0) is derived by

$$\Delta_{\lambda}/\sigma = \frac{|\Delta_{\lambda}|}{\sigma_{\lambda}}. \quad (12)$$

We assume that the systematic bias of λ is significant when $\Delta_{\lambda}/\sigma > 1$.

We also use the Jensen-Shannon divergence (JSD) as an auxiliary method to quantify the systematic bias for GW event analysis, which is a commonly used metric

to quantify the difference (or similarity) of two distributions [127]. Consider two one-dimensional marginalized posteriors $p(\lambda)$ and $q(\lambda)$, the JSD between them is given by

$$D_{JS}(p, q) = \frac{D_{KL}(p\|m) + D_{KL}(q\|m)}{2}, \quad (13)$$

where $m = (p + q)/2$, and D_{KL} is the Kullback–Leibler divergence,

$$D_{KL}(p\|q) = \int d\lambda p(\lambda) \log \frac{p(\lambda)}{q(\lambda)}. \quad (14)$$

The units of D_{JS} and D_{KL} correspond to the base of the logarithm (e.g., **bits** for the base of 2 and **nats** for the base of e). In this work, D_{JS} is computed from one-dimensional marginalized posteriors of eccentricity and reported in **bits**, using a Gaussian kernel density estimator implemented in `scipy` [128]. Following [6, 84, 124], we consider a JSD of 0.002 **bits** as the expected stochastic variation from the nested sampling, while a JSD larger than 0.007 **bits** suggests a significant bias between the compared distributions.

III. ANALYSIS OF ECCENTRIC GW CANDIDATES

A. Event Selection and Parameter Space

We select six eccentric candidates: GW190521, GW190620, GW190701, GW191109, GW200129, and GW200208_222617. Each has been reported to support the eccentric-BBH hypothesis in at least one study [80–85]. These events span a broad range of parameter space: detector-frame (source-frame) total masses M between 75 (63) M_{\odot} and 243 (153) M_{\odot} ; mass ratios q from 1.17 to 4.66; initial eccentricities at adopted f_{ref} , e_0 , from ≥ 0.1 up to 0.69; and network SNRs from 7.4 to 26.8. We use publicly available strain and PSD data from the Gravitational Wave Open Science Center (GWOSC) for parameter estimation [129]. For GW events affected by glitches, we use the glitch-mitigated data products released by GWOSC [130, 131]. Specifically, GW190701 and GW191109 use the BayesWave glitch modeling [132], and GW200129 uses the gwsubTRACT linear subtraction [133, 134].

B. Settings for Analysis of Eccentric Candidates

For all events except GW190521, parameters are specified at reference frequency $f_{\text{ref}} = 10$ Hz, which is also the starting frequency for waveform generation. Following [80, 86, 90], for GW190521, $f_{\text{ref}} = 5.5$ Hz to ensure all waveform modes are in band at the likelihood minimum frequency $f_{\text{min}} = 11$ Hz. As presented in Tab. I, we adopt a detector-frame chirp mass prior \mathcal{M}^{det} and

an inverse mass ratio prior $1/q \in [0.05, 1]$ that are implemented via uniform priors in component masses. For each event, the prior range of \mathcal{M} is chosen based on the corresponding posterior samples released by GWOSC. In particular, following [90], we set $\mathcal{M}^{\text{det}} \in [60, 200] M_{\odot}$ for GW190521. The priors for the initial eccentricity and relative anomaly at reference frequency are uniformly distributed with $e_0 \in [0, 0.5]$, $\zeta_0 \in [0, 2\pi]$. Following [90], we set the luminosity distance prior to be proportional to d_L^2 with a range of $[10^2, 10^4]$ Mpc for all events except GW190521. For GW190521, we instead adopt a prior uniform in comoving volume. Other priors are chosen as in [5, 90]. We enable distance and time marginalization to reduce computational cost.

Each event is analyzed twice, once with SEOBNRv5EHM and once with SEOBNRv5E. Subsequently, we compare the resulting posteriors from the two runs to calculate the normalized systematic errors Δ_e/σ , the JSDs, and the Bayes factors $\log_{10} \mathcal{B}_{\text{HM}/22}$ between the HOM-included (HM) and HOM-excluded (22) hypotheses.

C. Results of Eccentric Candidates

Fig. 2 presents the one-dimensional marginalized posteriors of e_0 obtained with SEOBNRv5EHM and SEOBNRv5E. Tab. II lists the median eccentricities with 90% confidence interval and the MAP eccentricities, together with the corresponding normalized systematic errors, JSDs, and \log_{10} Bayes factors. Across all six events, the measured values and posteriors of eccentricity are consistent with previous studies using SEOBNRv4EHM and SEOBNRv5EHM [84, 89, 90]. Based on medians, we did not identify systematic biases in eccentricity attributable to the exclusion of HOMs. Notably, GW200129's $\Delta_e^{\text{MAP}}/\sigma$ (1.07) and JSD (0.013 **bits**) are beyond our thresholds for significant biases. However, its median-based normalized systematic error ($\Delta_e^{\text{Median}}/\sigma = 0.13$) is much smaller than the threshold. This event is noteworthy, but we do not consider the bias significant, as it does not show a measurable change in median eccentricities.

Event by event, neglecting HOMs leads to an increased median eccentricity for GW190521, GW190620, GW191109, and GW200208_222617, and a decreased one for the rest of the events. GW190521, GW191109, and GW200208_222617 exhibit an increased MAP eccentricity when HOMs are neglected, while the MAP eccentricity for the other three events decreases. GW200129 has the largest median-based normalized systematic error ($\Delta_e^{\text{Median}}/\sigma = 0.13$), MAP-based systematic error ($\Delta_e^{\text{MAP}}/\sigma = 1.07$), and the largest JSD (0.013 **bits**). This may be due to its relatively high SNR (26.8) or the glitch in its data. In contrast, GW190701 exhibits the lowest median-based systematic error $\Delta_e^{\text{Median}}/\sigma = 0.02$ and MAP-based systematic error ($\Delta_e^{\text{MAP}}/\sigma = 0.01$), which might be related to the railing posterior and

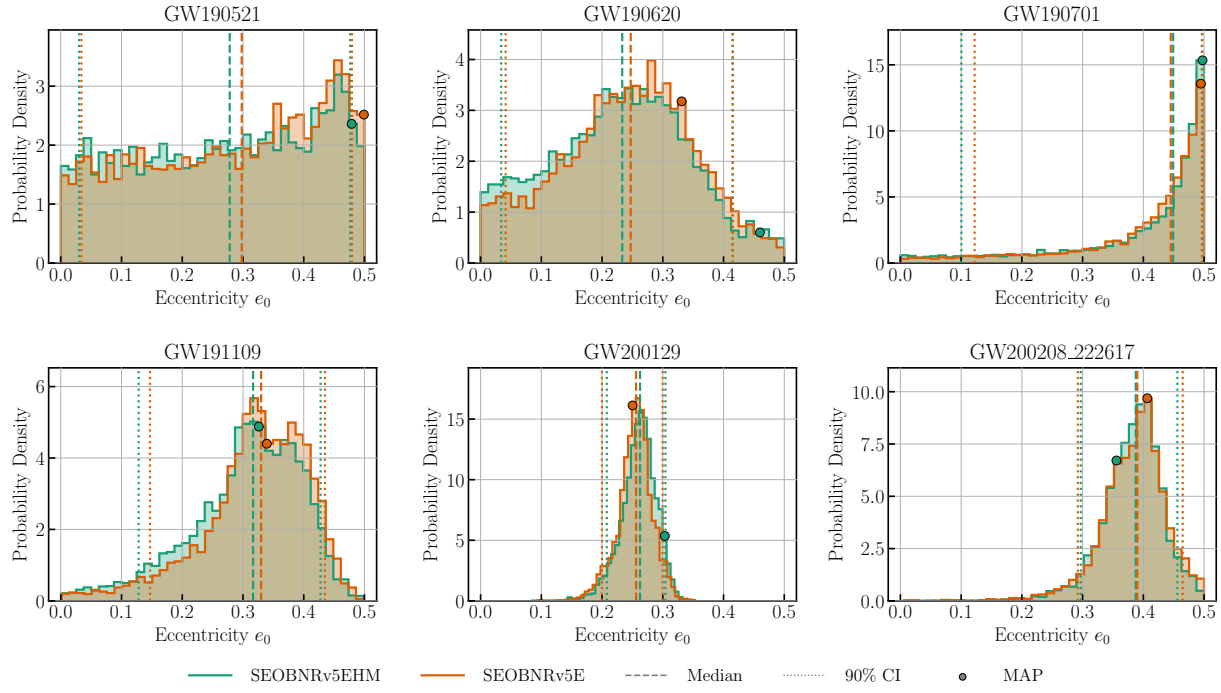


FIG. 2. Marginalized posterior distributions of initial eccentricity e_0 for all six GW events: GW190521, GW190620, GW190701, GW191109, GW200129, and GW200208_222617. Each panel presents the eccentricity posteriors obtained with SEOBNRv5EHM (green) and SEOBNRv5E (orange). Colored dashed lines represent the median eccentricities estimated, and colored circular markers denote the MAP point for each model. Colored dotted lines indicate the 90% credible interval of the eccentricity posteriors.

TABLE I. Priors used for GW event analysis.

Parameter	Prior Distribution	Prior Range
$\mathcal{M} (M_\odot)$	Uniform in Component Masses	depends on different events
$1/q$	Uniform in Component Masses	$[0.05, 1]$
e_0	Uniform	$[0.0, 0.5]$
ζ_0	Uniform	$[0, 2\pi]$
d_L (Mpc)	$\propto d_L^2$ ^a	$[10^2, 10^4]$
θ_{JN}	Sine	$[0, \pi]$
χ_1	AlignedSpin	$[-0.99, 0.99]$
χ_2	AlignedSpin	$[-0.99, 0.99]$
ϕ	Uniform	$[0, 2\pi]$
ψ	Uniform	$[0, \pi]$
R.A.	Uniform	$[0, 2\pi]$
Dec.	Cosine	$[-\pi/2, \pi/2]$
t_c (s)	Uniform	$[t^{\text{trigger}} - 0.1, t^{\text{trigger}} + 0.1]$

^a Uniform in comoving volume for GW190521

boundary effect that greatly suppresses the true systematic error. GW190521 yields the smallest JSD (0.001 bits) and small normalized systematic errors, consistent with its uninformative and prior-driven eccentricity posterior. $\log_{10} \mathcal{B}_{\text{HM/22}}$ are close to zero for all events, also indicating that including or omitting HOMs has little impact on estimated parameters. Most events

slightly prefer the HM hypothesis except for GW190620 and GW190701, which yield $\log_{10} \mathcal{B}_{\text{HM/22}} = -0.04$ and -0.29 , respectively. Consistent with Δ_e/σ and JSD, GW200129 holds the largest $\log_{10} \mathcal{B}_{\text{HM/22}}$ of 0.60.

In summary, the analysis of eccentric candidates reveals that none of the six events exhibits a significant systematic bias based on our joint criteria. In particular, for

TABLE II. Eccentricity measurement for each model and event. e_0^{Median} represent the median with 90% credible interval and e_0^{MAP} is the maximum a posteriori estimate of eccentricity, both specified at f_{ref} ; Δ_e/σ are the normalized systematic errors between SEOBNRv5EHM (HM) and SEOBNRv5E (22) based on both MAP and median; JSD denotes the Jensen-Shannon divergence between their eccentricity posteriors; and $\log_{10} \mathcal{B}_{\text{HM}/22}$ refers to the log-10 Bayes factors between the HOM-included (HM) and HOM-excluded (22) hypotheses.

Event	Model	e_0^{Median} (90% CI)	e_0^{MAP}	$\Delta_e^{\text{Median}}/\sigma$	$\Delta_e^{\text{MAP}}/\sigma$	JSD (bits)	$\log_{10} \mathcal{B}_{\text{HM}/22}$
GW190521	HM	$0.28^{+0.20}_{-0.25}$	0.48	0.09	0.05	0.001	0.19
	22	$0.30^{+0.18}_{-0.26}$	0.50				
GW190620	HM	$0.23^{+0.18}_{-0.20}$	0.46	0.07	0.69	0.003	-0.04
	22	$0.25^{+0.17}_{-0.21}$	0.33				
GW190701	HM	$0.45^{+0.05}_{-0.35}$	0.50	0.02	0.01	0.002	-0.29
	22	$0.45^{+0.05}_{-0.32}$	0.49				
GW191109	HM	$0.32^{+0.11}_{-0.19}$	0.33	0.09	0.09	0.006	0.41
	22	$0.33^{+0.11}_{-0.18}$	0.34				
GW200129	HM	$0.26^{+0.04}_{-0.05}$	0.30	0.13	1.07	0.013	0.60
	22	$0.26^{+0.04}_{-0.06}$	0.25				
GW200208_222617	HM	$0.39^{+0.07}_{-0.09}$	0.36	0.03	0.59	0.002	0.20
	22	$0.39^{+0.07}_{-0.10}$	0.41				

GW190521, we found no evidence of systematic biases in eccentricity estimation induced by omitting HOMs, suggesting that the exclusion of HOMs cannot explain the tension on its orbital eccentricity. In addition, to further validate the conclusion of the GW event analysis, we perform zero-noise injection studies based on the six events. The results support the conclusion drawn from our GW event analysis. Details of this verification are presented in Appendix A.

IV. INJECTION ANALYSIS

A. Settings for Injection Analysis

Although our analysis of the six GW events shows no clear evidence of significant systematic biases in eccentricity, we still need to determine under what conditions neglecting HOMs could significantly bias eccentricity measurements. To address this, we conduct an injection study over a grid of source parameters. The grid spans detector-frame total masses $M^{\text{det}} = \{100, 120, 140, 160\} M_{\odot}$ (Hereafter, unless otherwise specified, M refers to the detector-frame total mass); mass ratios $q = \{1, 2, 4, 6\}$; initial eccentricities at reference frequency ($f_{\text{ref}} = 10$ Hz) $e_0 = \{0, 0.3\}$; inclination angles $\theta_{\text{JN}} = \{0^\circ, 30^\circ, 60^\circ, 90^\circ\}$. We choose two network SNRs $\rho_{\text{mf}}^N = \{20, 50\}$ by adjusting the injected luminosity distance. ρ_{mf}^N is defined as

$$\rho_{\text{mf}}^N = \sqrt{(\rho_{\text{mf}}^L)^2 + (\rho_{\text{mf}}^H)^2 + (\rho_{\text{mf}}^V)^2}, \quad (15)$$

where ρ_{mf}^L , ρ_{mf}^H , and ρ_{mf}^V represent the matched filter SNR of LIGO (Livingston), LIGO (Hanford), and Virgo, respectively. We use the Advanced LIGO and Virgo PSD at design sensitivity.

These parameter choices are designed to explore how HOM-induced biases on eccentricity measurement change with different source properties. The effect of HOMs is more prominent for systems with highly asymmetric mass ratios and edge-on inclinations [91, 135]. Also, several studies have identified significant systematic bias for parameter estimation when neglecting HOMs in the high- M cases [91, 93]. Hence, we systematically vary the injected M , q , and θ_{JN} . In addition, because the influence of omitting HOMs may also depend on the true orbital eccentricity, we consider several injected eccentricities. The $e_0 = 0$ injections refer to quasi-circular systems and enable us to investigate whether omitting HOMs could lead to false claims of non-zero eccentricity for quasi-circular systems. By contrast, the $e_0 = 0.3$ cases are chosen as a representative value for the eccentricities estimated for the six GW events analyzed above, allowing us to quantify HOM-induced systematic biases for eccentric events. The reason for selecting different SNRs is that, although the absolute values of systematic errors are considered to be SNR-independent [92, 136], the normalized systematic errors can increase as the statistical errors are suppressed at high SNRs.

We employ SEOBNRv5EHM for injected signal generation and SEOBNRv5E for recovery, both with $f_{\text{ref}} = 10$ Hz, $f_{\text{min}} = 20$ Hz, and $f_{\text{max}} = 2048$ Hz for consistency with our analysis of eccentric candidates and

previous studies [90]. To isolate systematic error from potential error introduced by detector noise, we perform zero-noise injections. In this paper, we focus on the systematic biases of eccentricity induced by HOMs. Thus, we fix component spins to zero to avoid the spin effect on the parameter estimation.

We apply a detector-frame chirp mass prior $\mathcal{M}^{\text{det}} \in [5, 100] M_{\odot}$ and an inverse mass ratio prior $1/q \in [0.05, 1]$ that are uniformly sampled in component masses. The priors of the initial eccentricity and initial relative anomaly are uniformly distributed with a range of $e_0 \in [0, 0.5]$, $\zeta_0 \in [0, 2\pi]$. All the rest of the priors are identical to those adopted in our GW event analysis. We enable time, distance, and phase marginalization for computational efficiency. Tab. III presents the injected values and prior for each parameter.

B. Results for Injection Analysis

Figs. 3-4 show the normalized systematic error Δ_e/σ when HOMs are neglected in the GW waveforms. Red boxes mark the systems with $\Delta_e/\sigma > 1$. These results reveal that neglecting HOMs can raise non-negligible systematic biases in eccentricity. Based on medians, the biases are pronounced for high total masses ($M \gtrsim 120 M_{\odot}$), high mass ratios ($q \gtrsim 4$), large inclinations ($\theta_{\text{JN}} \gtrsim 30^\circ$), and high network SNRs ($\rho_{\text{mf}}^N \approx 20$ (for eccentric cases $\rho_{\text{mf}}^N \approx 50$)). This phenomenon generally vanishes for $M = 100 M_{\odot}$. Notably, red boxes frequently appear at $e_0 = 0$ for $M = \{140, 160\} M_{\odot}$. This suggests that, when analyzing quasi-circular systems with high total masses, high mass ratios, and large inclination angles, neglecting HOMs can lead to false-positive claims of eccentricity.

We identify several patterns from these results.

Relation between HOM-induced biases and total mass. Previous studies have reported significant HOM-induced systematic biases in parameter estimation for large M systems [91, 93], and our results are mostly consistent with such an opinion. As shown in Fig. 5, the normalized systematic error Δ_e/σ for the $M = 100 M_{\odot}$ and $M = 120 M_{\odot}$ cases is generally lower than that for $M = 140 M_{\odot}$ and $M = 160 M_{\odot}$. However, the absolute systematic error presents an oscillatory pattern, with decreased systematic biases in particular conditions (e.g., $e = 0.3$, $M = 140 M_{\odot}$ and $e = 0.0$, $M = 160 M_{\odot}$). One potential explanation for this phenomenon is that the systematic bias in eccentricity is related to the difference between injection and recovery waveforms. As HOMs become more prominent at larger total masses, the oscillation in phase would lead to an oscillatory behavior in waveform differences and hence a non-monotonic dependence of HOM-induced eccentricity bias on total mass. Other studies have also reported similar oscillatory patterns in systematic biases [77, 136, 137].

Relation between HOM-induced biases and mass asymmetry. As presented in Figs. 3-4 and Fig. 6,

there is a generally monotonic relation between mass ratios and HOM-induced eccentricity biases. For most systems with non-negligible systematic biases in eccentricity, larger mass ratios generally correspond to larger normalized systematic errors. This is consistent with our expectation, as HOMs become more prominent at higher mass ratios. However, there are certain circumstances in which the dependence of the eccentricity bias on mass ratios exhibits a similar oscillatory pattern as mentioned above (e.g., $M = 160 M_{\odot}$), as shown in the upper plot of Fig. 6.

Relation between HOM-induced biases and inclination angle. Roughly, Δ_e/σ increases with θ_{JN} for fixed $(M, q, \rho_{\text{mf}}^N)$. Fig. 7 compares a set of four eccentricity posteriors with the same injected parameters but different inclination angles, providing a clear view of how the biases vary with inclination angles. This naturally aligns with our expectation, as the HOMs are enhanced with larger inclination angles.

Relation between HOM-induced biases and orbital eccentricity. For systems with fixed (M, ρ_{mf}^N) , significant biases in eccentricity occur more frequently for quasi-circular cases than for eccentric ones. Furthermore, the largest normalized systematic error in eccentricity is observed at $e_0 = 0.0$ ($\Delta_e^{\text{Median}}/\sigma \approx 9.7$ at $(M, q, \theta_{\text{JN}}, \rho_{\text{mf}}^N) = (140 M_{\odot}, 6, 90^\circ, 50)$). This implies that, compared to eccentric systems, ignoring HOMs is more likely to yield spurious non-zero eccentricity in parameter estimation for quasi-circular binaries. This may partly result from the prior-boundary effect, as the true eccentricity $e_0 = 0.0$ falls on the lower edge of the eccentricity prior.

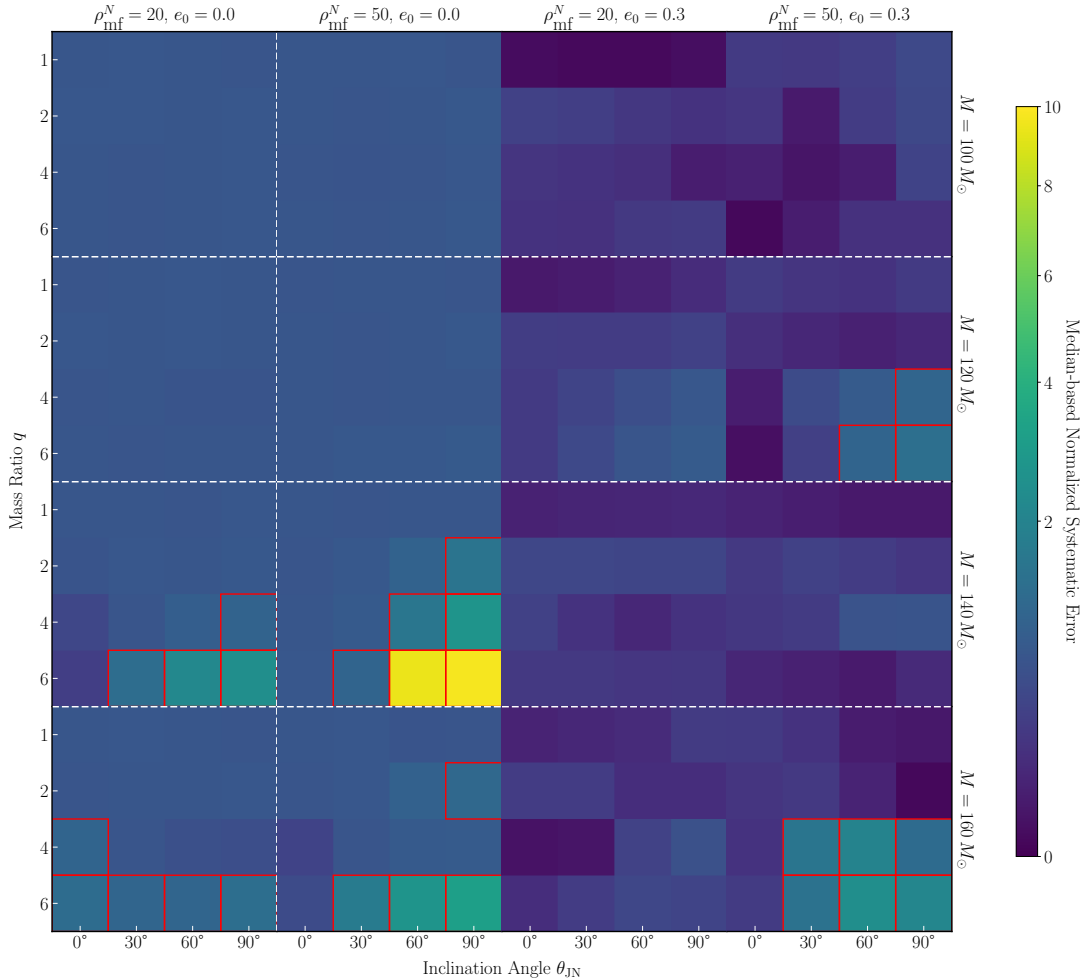
Relation between HOM-induced biases and network SNR. We note that the HOM-induced systematic biases in eccentricity are greater at higher network SNR. Figs. 5-7 show how increasing network SNRs amplify these biases. The absolute systematic errors change little with SNR, which is consistent with [92] and our expectation. Instead, higher SNR primarily reduces the statistical errors and, consequently, increases the normalized systematic errors in eccentricity estimation.

Finally, we find that for $M = 100 M_{\odot}$ systems, neglecting HOMs generally would not lead to significant systematic biases across the grid. This suggests that the dominant (2, 2) mode alone might be sufficient to constrain e_0 for low-mass systems of the sources specified in this study. This is consistent with our expectations, since parameter estimation for low-mass binaries is dominated by the long inspiral phase, where HOMs contribute much less than during the merger-ringdown.

For validation, we select two systems that exhibit large eccentricity biases when HOMs are neglected and perform additional injection-recovery studies using SEOBNRv5EHM for both injection and recovery. In particular, we choose $(M, q, e_0, \theta_{\text{JN}}, \rho_{\text{mf}}^N) = (140 M_{\odot}, 6, 0.0, 90^\circ, 50)$ and $(160 M_{\odot}, 6, 0.3, 90^\circ, 50)$, for which $\Delta_e^{\text{Median}}/\sigma \approx 9.7$ and 2.1, respectively, when HOMs are omitted. In both cases, the injected parame-

TABLE III. Injected values and priors of parameters for injection studies.

Parameter	Injected Values	Prior Distribution	Prior Range
$M (M_\odot)$	100, 120, 140, 160	–	–
$\mathcal{M} (M_\odot)$	–	Uniform in Component Masses	[5, 100]
$1/q$	1, 1/2, 1/4, 1/6	Uniform in Component Masses	[0.05, 1]
e_0	0, 0.3	Uniform	[0.0, 0.5]
ζ_0	0	Uniform	[0, 2π]
d_L (Mpc)	depends on different events	$\propto d_L^2$	[10^2 , 10^4]
θ_{JN}	$0^\circ, 30^\circ, 60^\circ, 90^\circ$	Sine	[0, π]
ϕ	0	Uniform	[0, 2π]
ψ	0	Uniform	[0, π]
R.A.	2.2	Uniform	[0, 2π]
Dec.	-1.25	Cosine	[- $\pi/2$, $\pi/2$]
t_c (s)	1126259642.413	Uniform	[1126259642.313, 1126259642.513]

FIG. 3. Median-based normalized systematic errors Δ_e/σ for all injection analyses. Rows compare results with different total masses, and columns compare results with different network SNRs and eccentricities. The block colors correspond to the values of normalized Δ_e/σ . Every block with $\Delta_e/\sigma > 1$ is marked with a red box.

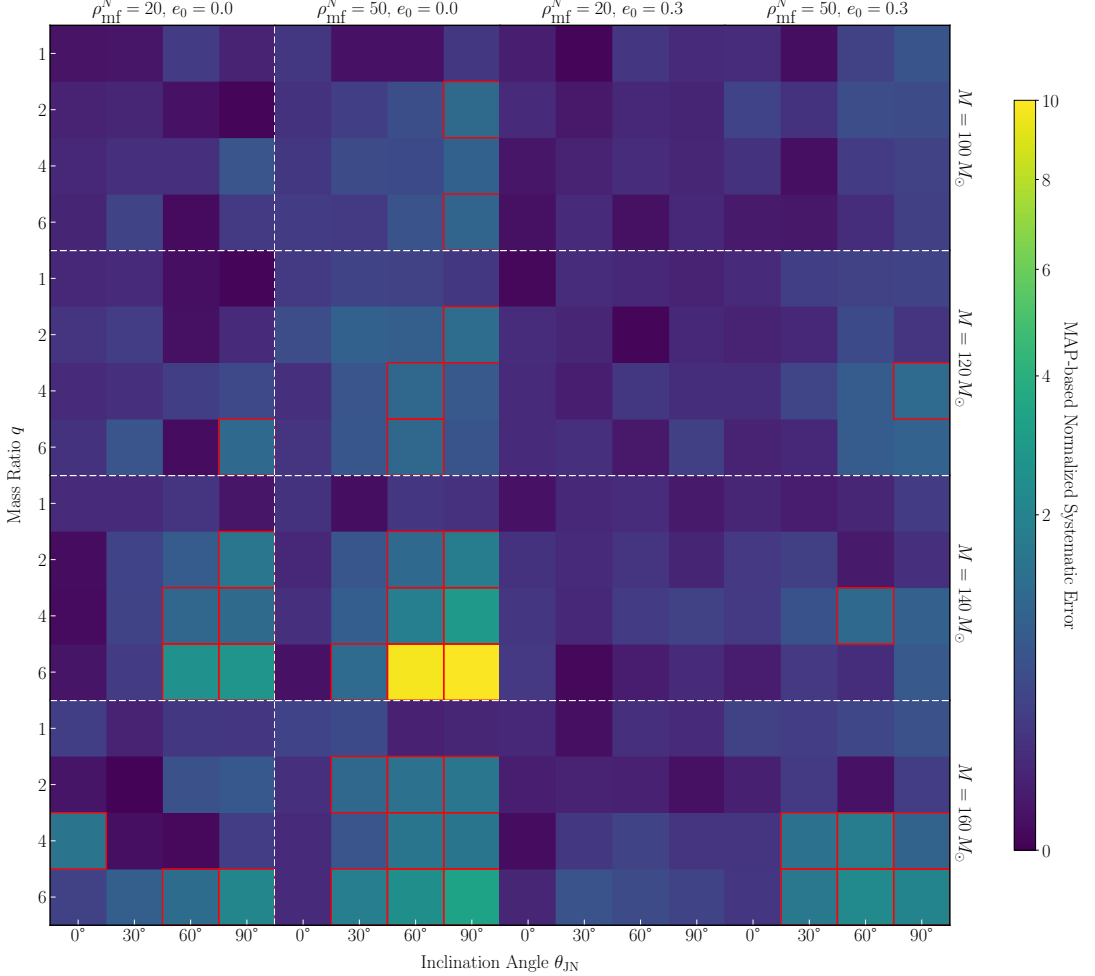


FIG. 4. The same as in Fig. 3 but for normalized systematic errors calculated using MAP.

ter values are accurately recovered, validating our analysis pipeline. The left plot of Fig. 1 presents the recovered eccentricity posterior at $(M, q, e_0, \theta_{\text{JN}}, \rho_{\text{mf}}^N) = (160M_{\odot}, 6, 0.3, 90^\circ, 50)$ when HOMs are included in PE.

V. CONCLUSION AND DISCUSSION

In this work, we investigate the systematic biases in the measurement of the orbital eccentricity of binary black holes that are introduced by neglecting higher-order modes in the gravitational-wave waveforms. We perform Bayesian inference with `bilby` and the spin-aligned eccentric IMR waveform model SEOBNRv5EHM. We quantify the biases using two metrics, including the MAP/median-based normalized systematic errors Δ_e/σ and the Jensen-Shannon divergence in **bits**.

In Sec. III, we analyze six GW events using SEOBNRv5EHM and its HOM-excluded counterpart SEOBNRv5E, and compare the eccentricity posteriors obtained with the two models. We find no evidence of significant

HOM-induced systematic biases ($\Delta_e/\sigma > 1$) in eccentricity. Although GW200129 exhibits a MAP-based normalized systematic error $\Delta_e^{\text{MAP}}/\sigma$ of 1.07 and a JSD of 0.013 **bits**, its median eccentricity is mostly not affected by ignoring HOMs, with $\Delta_e^{\text{Median}}/\sigma = 0.13$. Notably, the HOM-induced eccentricity bias of GW190521 is very small, suggesting that the ignorance of HOMs is insufficient to explain the tension of eccentricity measurement for GW190521. The discrepancy between different studies might be due to the choice of priors, waveform model errors, parameter estimation methods, or other unknown effects.

In Sec. IV, we present zero-noise injection studies to search for parameter regions where HOM-induced biases in eccentricity are non-negligible ($\Delta_e/\sigma > 1$). We inject simulated GW signals using SEOBNRv5EHM and recover parameters using SEOBNRv5E, varying total mass, mass ratio, eccentricity, inclination angle, and network SNR. According to the results, neglecting HOMs could raise significant biases in eccentricity, which are prominent for systems characterized by large total masses ($M \gtrsim 120M_{\odot}$), highly asymmetric mass ratios ($q \gtrsim 4$),

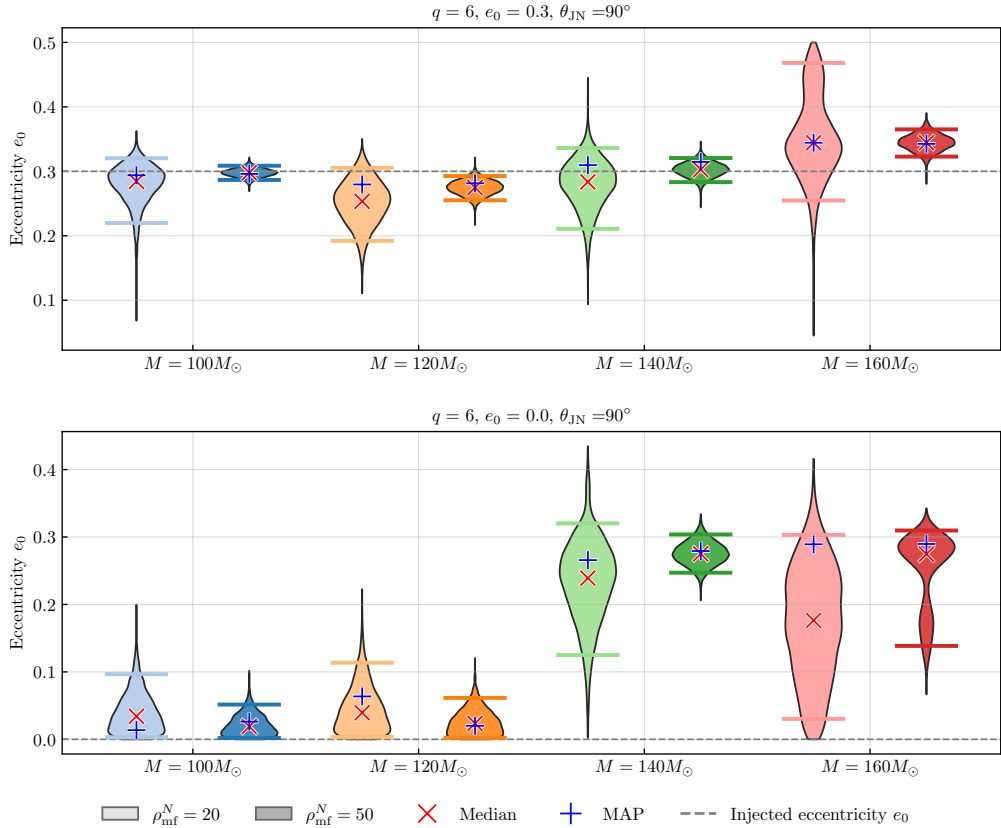


FIG. 5. Eccentricity posteriors recovered with HOM-excluded SEOBNRv5E for injections generated with HOM-included SEOBNRv5EHM. We show results for systems with different total masses M and compare two network matched-filter SNRs, $\rho_{\text{mf}}^N = 20$ (lighter color) and $\rho_{\text{mf}}^N = 50$ (darker color). The top panel presents the case of $e_0 = 0.3$, $q = 2$, and $\theta_{\text{JN}} = 90^\circ$; the bottom panel presents the case of $e_0 = 0.0$, $q = 2$, and $\theta_{\text{JN}} = 90^\circ$. The gray dashed lines indicate injected values of eccentricity, and the colored solid lines represent the 90% credible interval of each corresponding eccentricity posteriors. The median and MAP eccentricities are marked with red crosses and blue plus signs, respectively.

large inclinations ($\theta_{\text{JN}} \gtrsim 30^\circ$), and high SNR ($\rho_{\text{mf}}^N \approx 50$). Notably, quasi-circular BBHs in this parameter region can yield false-positive claims of eccentricity when analyzed with HOM-excluding models. Therefore, to avoid systematic biases and false positives in eccentricity measurement, HOMs should be included in future data analysis.

There are several limitations to our study. First, due to waveform availability, we only compared HOM-included and HOM-excluded spin-aligned eccentric waveform models, without taking spin-precession into account. As pointed out in Romero-Shaw *et al.* [80], there is a degeneracy between spin-precession and eccentricity. Second, due to the computational cost of SEOBNRv5EHM, we employ a parameter grid with limited resolution and coverage. A finer and broader grid search over these parameters would be necessary to draw a more comprehensive conclusion. Lastly, we adopt only one waveform model, which is based on the EOB formalism. It is worthwhile to compare HOM-induced eccentricity biases between different eccentric models (e.g., the phenomenological eccentric model IMRPhenomTEHM [119])

for the robustness of the conclusion. In addition, the HOM-induced biases for third-generation ground-based GW detectors such as ET and CT, as well as space-based detectors LISA, Taiji, and TianQin, deserve in-depth study, as they are expected to operate with much higher sensitivity and a lower observing band than current detectors. We leave this for future research.

VI. ACKNOWLEDGMENT

We would like to thank Zhoujian Cao, Aldo Gamboa, Alexander Nitz, Shichao Wu, Keisi Kacanja, Kanchan Soni, Divyajyoti, Gareth Cabourn Davies, Tom Dent, and Yuxuan Li for their helpful discussion. We also thank Colm Talbot for assistance with BILBY.

This work is supported by the National Natural Science Foundation of China Grants No. 12575063, and in part by “the Special Funds for the Double First-Class Development of Wuhan University” under the reference No. 2025-1302-010. The numerical calculations in this paper have been done on the supercomputing system in the Su-

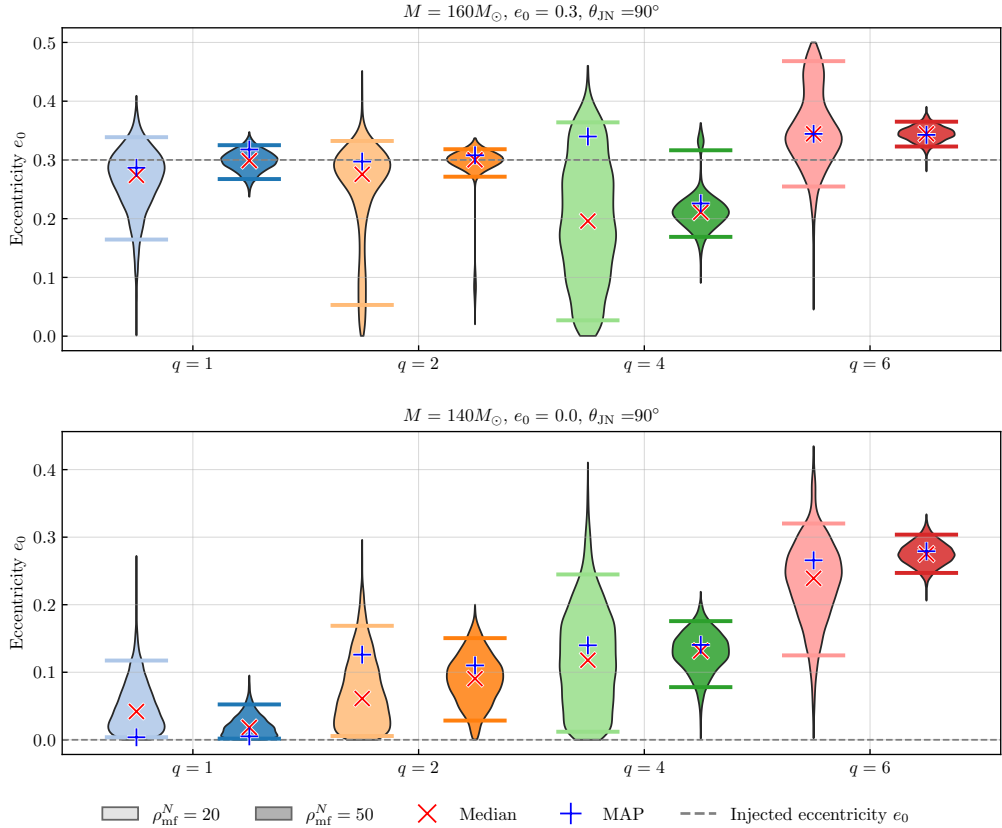


FIG. 6. The same as in Fig. 5 but for systems with different mass ratios q . The top panel presents the case of $M = 160M_{\odot}$, $e_0 = 0.3$, and $\theta_{\text{JN}} = 90^\circ$; the bottom panel presents the case of $M = 140M_{\odot}$, $e_0 = 0.0$, and $\theta_{\text{JN}} = 90^\circ$.

percomputing Center of Wuhan University. Some of the results in this paper have been derived using the “pesummary” package [138]. This research has made use of data or software obtained from the Gravitational Wave Open Science Center (gwosc.org), a service of the LIGO Scientific Collaboration, the Virgo Collaboration, and KAGRA.

Appendix A: Verification of Analysis of Eccentric Candidates

Event	190521	190620	190701	191109	200129	200208
$\Delta_e^{\text{Median}}/\sigma$	0.00	0.01	0.03	0.18	0.02	0.02
$\Delta_e^{\text{MAP}}/\sigma$	0.18	0.66	0.24	0.31	0.63	0.18
JSD (bits)	0.000	0.001	0.001	0.009	0.001	0.001
$\log_{10} \mathcal{B}_{\text{HM}/22}$	-0.55	-0.09	-0.12	-0.22	-0.22	-0.08

TABLE IV. The results of event-based injections, including the normalized systematic error of eccentricity for median and MAP, the Jensen-Shannon divergence, and the log-10 Bayes factors between the HOM-included (HM) and HOM-excluded (22) hypotheses.

We perform event-based injection studies to verify the conclusion of the GW event analysis. First, we use SEOBNRv5EHM to generate simulated GW signals with median parameters of each event obtained in GW event analysis using SEOBNRv5EHM. Next, we inject the signals into zero-noise detectors while using the same PSDs as those in GW event analysis, and recover parameters with the identical settings of GW event analysis using both SEOBNRv5EHM and SEOBNRv5E. Finally, we compare the results of the injection study and the GW event analysis to verify our conclusion.

The results are shown in Tab. IV and Fig. 8. The event-based injections yield conclusions that omitting HOMs does not lead to significant biases in eccentricity measurement, which is consistent with our GW event analysis. Notably, GW191109-like injection exhibits a JSD of 0.009 bits that is beyond its threshold for significant biases. Nevertheless, the measured eccentricity, both for median and MAP, of this injection is not significantly biased.

Notably, the eccentricity posteriors of GW190521, GW190701, and GW200208_222617 in event-based injections are significantly different from those of the GW event analysis. This is not beyond our expectations due to the uninformative eccentricity posterior for

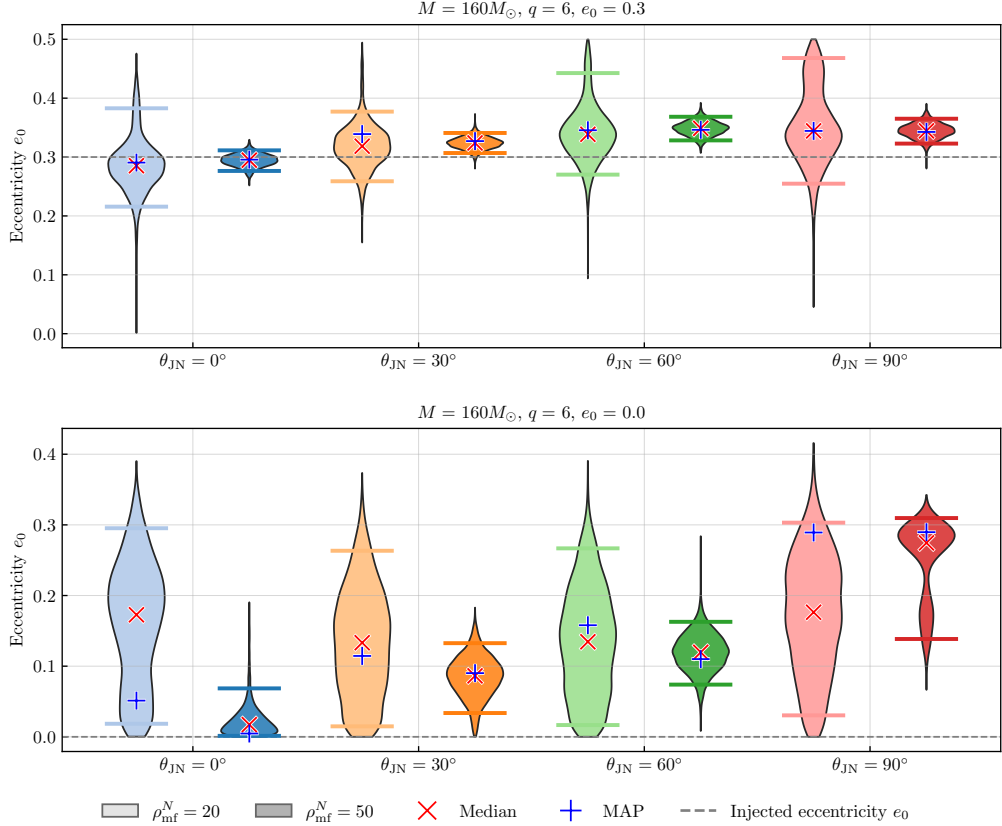


FIG. 7. The same as in Fig. 5 but for systems with different inclination angles θ_{JN} . The top panel presents the case of $M = 160M_{\odot}$, $q = 6$, and $e_0 = 0.3$; the bottom panel presents the case of $M = 160M_{\odot}$, $q = 6$, and $e_0 = 0.0$.

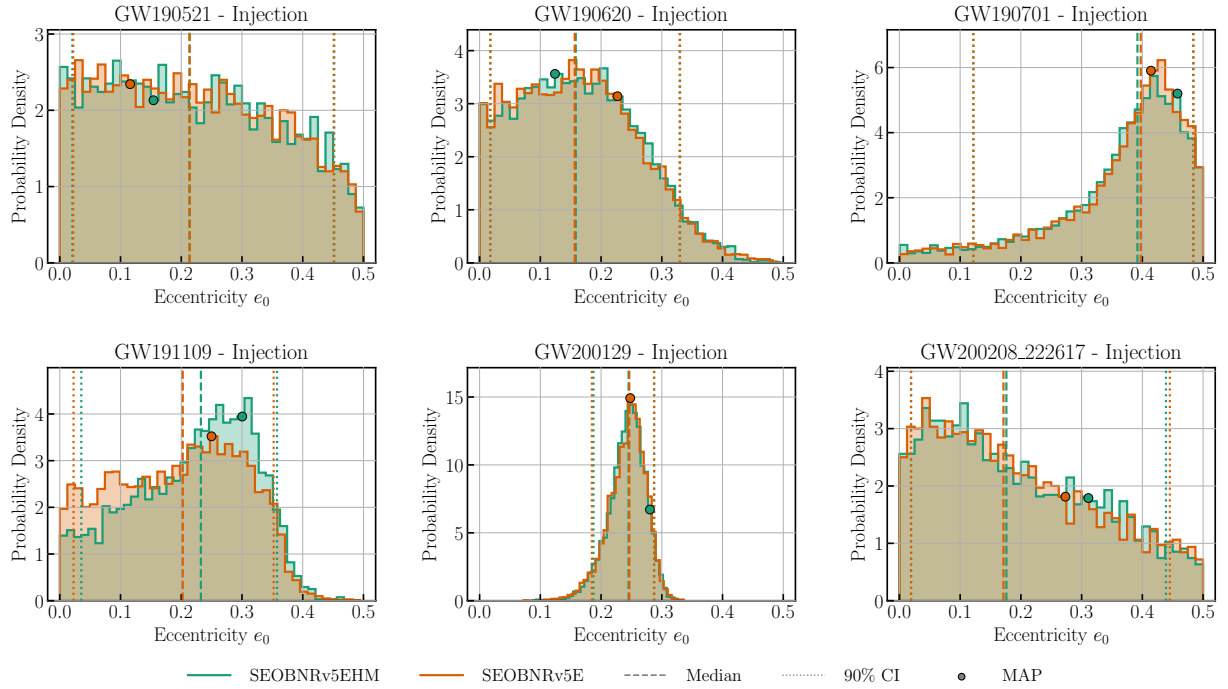


FIG. 8. The same as in Fig. 2 but for event-based injection studies.

GW190521, the railing posterior for GW190701, and the relatively low network SNR for GW200208_222617. Moreover, the GW190521-like injection exhibits a badly converged eccentricity posterior. This also suggests

an important implication: The orbital eccentricity of GW190521-like events may not be accurately constrained with the current sensitivity of LIGO and Virgo.

[1] B. P. Abbott *et al.* (LIGO Scientific, Virgo), Observation of Gravitational Waves from a Binary Black Hole Merger, *Phys. Rev. Lett.* **116**, 061102 (2016), [arXiv:1602.03837 \[gr-qc\]](https://arxiv.org/abs/1602.03837).

[2] J. Aasi *et al.* (LIGO Scientific), Advanced LIGO, *Class. Quant. Grav.* **32**, 074001 (2015), [arXiv:1411.4547 \[gr-qc\]](https://arxiv.org/abs/1411.4547).

[3] F. Acernese *et al.* (VIRGO), Advanced Virgo: a second-generation interferometric gravitational wave detector, *Class. Quant. Grav.* **32**, 024001 (2015), [arXiv:1408.3978 \[gr-qc\]](https://arxiv.org/abs/1408.3978).

[4] Y. Aso, Y. Michimura, K. Somiya, M. Ando, O. Miyakawa, T. Sekiguchi, D. Tatsumi, and H. Yamamoto (KAGRA), Interferometer design of the KAGRA gravitational wave detector, *Phys. Rev. D* **88**, 043007 (2013), [arXiv:1306.6747 \[gr-qc\]](https://arxiv.org/abs/1306.6747).

[5] B. P. Abbott *et al.* (LIGO Scientific, Virgo), GWTC-1: A Gravitational-Wave Transient Catalog of Compact Binary Mergers Observed by LIGO and Virgo during the First and Second Observing Runs, *Phys. Rev. X* **9**, 031040 (2019), [arXiv:1811.12907 \[astro-ph.HE\]](https://arxiv.org/abs/1811.12907).

[6] R. Abbott *et al.* (LIGO Scientific, Virgo), GWTC-2: Compact Binary Coalescences Observed by LIGO and Virgo During the First Half of the Third Observing Run, *Phys. Rev. X* **11**, 021053 (2021), [arXiv:2010.14527 \[gr-qc\]](https://arxiv.org/abs/2010.14527).

[7] R. Abbott *et al.* (LIGO Scientific, VIRGO), GWTC-2.1: Deep extended catalog of compact binary coalescences observed by LIGO and Virgo during the first half of the third observing run, *Phys. Rev. D* **109**, 022001 (2024), [arXiv:2108.01045 \[gr-qc\]](https://arxiv.org/abs/2108.01045).

[8] A. G. Abac *et al.* (LIGO Scientific, VIRGO, KAGRA), GWTC-4.0: Updating the Gravitational-Wave Transient Catalog with Observations from the First Part of the Fourth LIGO-Virgo-KAGRA Observing Run (2025), [arXiv:2508.18082 \[gr-qc\]](https://arxiv.org/abs/2508.18082).

[9] B. F. Schutz, Determining the Hubble Constant from Gravitational Wave Observations, *Nature* **323**, 310 (1986).

[10] B. P. Abbott *et al.* (LIGO Scientific, Virgo, 1M2H, Dark Energy Camera GW-E, DES, DLT40, Las Cumbres Observatory, VINROUGE, MASTER), A gravitational-wave standard siren measurement of the Hubble constant, *Nature* **551**, 85 (2017), [arXiv:1710.05835 \[astro-ph.CO\]](https://arxiv.org/abs/1710.05835).

[11] M. Soares-Santos *et al.* (DES, LIGO Scientific, Virgo), First Measurement of the Hubble Constant from a Dark Standard Siren using the Dark Energy Survey Galaxies and the LIGO/Virgo Binary-Black-hole Merger GW170814, *Astrophys. J. Lett.* **876**, L7 (2019), [arXiv:1901.01540 \[astro-ph.CO\]](https://arxiv.org/abs/1901.01540).

[12] R. Abbott *et al.* (LIGO Scientific, Virgo, KAGRA), Constraints on the Cosmic Expansion History from GWTC-3, *Astrophys. J.* **949**, 76 (2023), [arXiv:2111.03604 \[astro-ph.CO\]](https://arxiv.org/abs/2111.03604).

[13] A. G. Abac *et al.* (LIGO Scientific, VIRGO, KAGRA), GWTC-4.0: Constraints on the Cosmic Expansion Rate and Modified Gravitational-wave Propagation (2025), [arXiv:2509.04348 \[astro-ph.CO\]](https://arxiv.org/abs/2509.04348).

[14] B. P. Abbott *et al.* (LIGO Scientific, Virgo), Binary Black Hole Population Properties Inferred from the First and Second Observing Runs of Advanced LIGO and Advanced Virgo, *Astrophys. J. Lett.* **882**, L24 (2019), [arXiv:1811.12940 \[astro-ph.HE\]](https://arxiv.org/abs/1811.12940).

[15] R. Abbott *et al.* (LIGO Scientific, Virgo), Population Properties of Compact Objects from the Second LIGO-Virgo Gravitational-Wave Transient Catalog, *Astrophys. J. Lett.* **913**, L7 (2021), [arXiv:2010.14533 \[astro-ph.HE\]](https://arxiv.org/abs/2010.14533).

[16] R. Abbott *et al.* (KAGRA, VIRGO, LIGO Scientific), Population of Merging Compact Binaries Inferred Using Gravitational Waves through GWTC-3, *Phys. Rev. X* **13**, 011048 (2023), [arXiv:2111.03634 \[astro-ph.HE\]](https://arxiv.org/abs/2111.03634).

[17] A. G. Abac *et al.* (LIGO Scientific, VIRGO, KAGRA), GWTC-4.0: Population Properties of Merging Compact Binaries (2025), [arXiv:2508.18083 \[astro-ph.HE\]](https://arxiv.org/abs/2508.18083).

[18] C. M. Will, The Confrontation between General Relativity and Experiment, *Living Rev. Rel.* **17**, 4 (2014), [arXiv:1403.7377 \[gr-qc\]](https://arxiv.org/abs/1403.7377).

[19] B. P. Abbott *et al.* (LIGO Scientific, Virgo), Tests of general relativity with GW150914, *Phys. Rev. Lett.* **116**, 221101 (2016), [Erratum: *Phys. Rev. Lett.* 121, 129902 (2018)], [arXiv:1602.03841 \[gr-qc\]](https://arxiv.org/abs/1602.03841).

[20] B. P. Abbott *et al.* (LIGO Scientific, Virgo), Tests of General Relativity with GW170817, *Phys. Rev. Lett.* **123**, 011102 (2019), [arXiv:1811.00364 \[gr-qc\]](https://arxiv.org/abs/1811.00364).

[21] B. P. Abbott *et al.* (LIGO Scientific, Virgo), Tests of General Relativity with the Binary Black Hole Signals from the LIGO-Virgo Catalog GWTC-1, *Phys. Rev. D* **100**, 104036 (2019), [arXiv:1903.04467 \[gr-qc\]](https://arxiv.org/abs/1903.04467).

[22] R. Abbott *et al.* (LIGO Scientific, Virgo), Tests of general relativity with binary black holes from the second LIGO-Virgo gravitational-wave transient catalog, *Phys. Rev. D* **103**, 122002 (2021), [arXiv:2010.14529 \[gr-qc\]](https://arxiv.org/abs/2010.14529).

[23] R. Abbott *et al.* (LIGO Scientific, VIRGO, KAGRA), Tests of General Relativity with GWTC-3 (2021), [arXiv:2112.06861 \[gr-qc\]](https://arxiv.org/abs/2112.06861).

[24] N. V. Krishnendu and F. Ohme, Testing General Relativity with Gravitational Waves: An Overview, *Universe* **7**, 497 (2021), [arXiv:2201.05418 \[gr-qc\]](https://arxiv.org/abs/2201.05418).

[25] T. L. S. Collaboration, the Virgo Collaboration, and the KAGRA Collaboration, Black hole spectroscopy and tests of general relativity with gw250114 (2025), [arXiv:2509.08099 \[gr-qc\]](https://arxiv.org/abs/2509.08099).

[26] A. G. Abac *et al.* (LIGO Scientific, Virgo, KAGRA), GW250114: Testing Hawking’s Area Law and the Kerr Nature of Black Holes, *Phys. Rev. Lett.* **135**, 111403 (2025), [arXiv:2509.08054 \[gr-qc\]](https://arxiv.org/abs/2509.08054).

[27] K. Belczynski, V. Kalogera, and T. Bulik, A Comprehensive study of binary compact objects as grav-

itational wave sources: Evolutionary channels, rates, and physical properties, *Astrophys. J.* **572**, 407 (2001), [arXiv:astro-ph/0111452](#).

[28] C. L. Rodriguez, M. Zevin, C. Pankow, V. Kalogera, and F. A. Rasio, Illuminating Black Hole Binary Formation Channels with Spins in Advanced LIGO, *Astrophys. J. Lett.* **832**, L2 (2016), [arXiv:1609.05916](#) [astro-ph.HE].

[29] I. Mandel and R. O’Shaughnessy, Compact Binary Coalescences in the Band of Ground-based Gravitational-Wave Detectors, *Class. Quant. Grav.* **27**, 114007 (2010), [arXiv:0912.1074](#) [astro-ph.HE].

[30] I. Kowalska, T. Bulik, K. Belczynski, M. Dominik, and D. Gondek-Rosinska, The eccentricity distribution of compact binaries, *Astron. Astrophys.* **527**, A70 (2011), [arXiv:1010.0511](#) [astro-ph.CO].

[31] H. A. Bethe and G. E. Brown, Evolution of binary compact objects which merge, *Astrophys. J.* **506**, 780 (1998), [arXiv:astro-ph/9802084](#).

[32] S. Stevenson, A. Vigna-Gómez, I. Mandel, J. W. Barrett, C. J. Neijssel, D. Perkins, and S. E. de Mink, Formation of the first three gravitational-wave observations through isolated binary evolution, *Nature Commun.* **8**, 14906 (2017), [arXiv:1704.01352](#) [astro-ph.HE].

[33] K. Belczynski, A. Buonanno, M. Cantiello, C. L. Fryer, D. E. Holz, I. Mandel, M. C. Miller, and M. Walczak, The Formation and Gravitational-Wave Detection of Massive Stellar Black-Hole Binaries, *Astrophys. J.* **789**, 120 (2014), [arXiv:1403.0677](#) [astro-ph.HE].

[34] M. Mapelli, Binary Black Hole Mergers: Formation and Populations, *Front. Astron. Space Sci.* **7**, 38 (2020), [arXiv:2105.12455](#) [astro-ph.HE].

[35] Y. Bouffanais, M. Mapelli, F. Santoliquido, N. Giacobbo, U. N. Di Carlo, S. Rastello, M. C. Artale, and G. Iorio, New insights on binary black hole formation channels after GWTC-2: young star clusters versus isolated binaries, *Mon. Not. Roy. Astron. Soc.* **507**, 5224 (2021), [arXiv:2102.12495](#) [astro-ph.HE].

[36] M. Livio and N. Soker, The Common Envelope Phase in the Evolution of Binary Stars, *Astrophys. J.* **329**, 764 (1988).

[37] N. Ivanova *et al.*, Common Envelope Evolution: Where we stand and how we can move forward, *Astron. Astrophys. Rev.* **21**, 59 (2013), [arXiv:1209.4302](#) [astro-ph.HE].

[38] K. Belczynski, D. E. Holz, T. Bulik, and R. O’Shaughnessy, The first gravitational-wave source from the isolated evolution of two 40-100 Msun stars, *Nature* **534**, 512 (2016), [arXiv:1602.04531](#) [astro-ph.HE].

[39] P. Marchant, N. Langer, P. Podsiadlowski, T. M. Tauris, and T. J. Moriya, A new route towards merging massive black holes, *Astron. Astrophys.* **588**, A50 (2016), [arXiv:1601.03718](#) [astro-ph.SR].

[40] P. C. Peters, Gravitational Radiation and the Motion of Two Point Masses, *Phys. Rev.* **136**, B1224 (1964).

[41] S. Sigurdsson and L. Hernquist, Primordial black holes in globular clusters, *Nature* **364**, 423 (1993).

[42] S. F. Portegies Zwart and S. McMillan, Black hole mergers in the universe, *Astrophys. J. Lett.* **528**, L17 (2000), [arXiv:astro-ph/9910061](#).

[43] M. Zevin, S. S. Bavera, C. P. L. Berry, V. Kalogera, T. Fragos, P. Marchant, C. L. Rodriguez, F. Antonini, D. E. Holz, and C. Pankow, One Channel to Rule Them All? Constraining the Origins of Binary Black Holes Using Multiple Formation Pathways, *Astrophys. J.* **910**, 152 (2021), [arXiv:2011.10057](#) [astro-ph.HE].

[44] R. M. O’Leary, B. Kocsis, and A. Loeb, Gravitational waves from scattering of stellar-mass black holes in galactic nuclei, *Mon. Not. Roy. Astron. Soc.* **395**, 2127 (2009), [arXiv:0807.2638](#) [astro-ph].

[45] B. Kocsis and J. Levin, Repeated Bursts from Relativistic Scattering of Compact Objects in Galactic Nuclei, *Phys. Rev. D* **85**, 123005 (2012), [arXiv:1109.4170](#) [astro-ph.CO].

[46] L. Gondán, B. Kocsis, P. Raffai, and Z. Frei, Eccentric Black Hole Gravitational-Wave Capture Sources in Galactic Nuclei: Distribution of Binary Parameters, *Astrophys. J.* **860**, 5 (2018), [arXiv:1711.09989](#) [astro-ph.HE].

[47] J. Samsing, M. MacLeod, and E. Ramirez-Ruiz, The Formation of Eccentric Compact Binary Inspirals and the Role of Gravitational Wave Emission in Binary-Single Stellar Encounters, *Astrophys. J.* **784**, 71 (2014), [arXiv:1308.2964](#) [astro-ph.HE].

[48] J. Samsing and E. Ramirez-Ruiz, On the Assembly Rate of Highly Eccentric Binary Black Hole Mergers, *Astrophys. J. Lett.* **840**, L14 (2017), [arXiv:1703.09703](#) [astro-ph.HE].

[49] E. Michaely and H. B. Perets, Gravitational-wave Sources from Mergers of Binary Black Holes Catalyzed by Flyby Interactions in the Field, *Astrophys. J. Lett.* **887**, L36 (2019), [arXiv:1902.01864](#) [astro-ph.SR].

[50] R. M. O’Leary, F. A. Rasio, J. M. Fregeau, N. Ivanova, and R. W. O’Shaughnessy, Binary mergers and growth of black holes in dense star clusters, *Astrophys. J.* **637**, 937 (2006), [arXiv:astro-ph/0508224](#).

[51] B. McKernan *et al.*, Constraining Stellar-mass Black Hole Mergers in AGN Disks Detectable with LIGO, *Astrophys. J.* **866**, 66 (2018), [arXiv:1702.07818](#) [astro-ph.HE].

[52] Y. Yang, I. Bartos, Z. Haiman, B. Kocsis, Z. Marka, N. C. Stone, and S. Marka, AGN Disks Harden the Mass Distribution of Stellar-mass Binary Black Hole Mergers, *Astrophys. J.* **876**, 122 (2019), [arXiv:1903.01405](#) [astro-ph.HE].

[53] J. Samsing, Eccentric Black Hole Mergers Forming in Globular Clusters, *Phys. Rev. D* **97**, 103014 (2018), [arXiv:1711.07452](#) [astro-ph.HE].

[54] M. Zevin, J. Samsing, C. Rodriguez, C.-J. Haster, and E. Ramirez-Ruiz, Eccentric Black Hole Mergers in Dense Star Clusters: The Role of Binary–Binary Encounters, *Astrophys. J.* **871**, 91 (2019), [arXiv:1810.00901](#) [astro-ph.HE].

[55] L. Gondán and B. Kocsis, Measurement Accuracy of Inspiring Eccentric Neutron Star and Black Hole Binaries Using Gravitational Waves, *Astrophys. J.* **871**, 178 (2019), [arXiv:1809.00672](#) [astro-ph.HE].

[56] Y. Kozai, Secular perturbations of asteroids with high inclination and eccentricity, *Astron. J.* **67**, 591 (1962).

[57] M. L. Lidov, The evolution of orbits of artificial satellites of planets under the action of gravitational perturbations of external bodies, *Planet. Space Sci.* **9**, 719 (1962).

[58] F. Antonini and H. B. Perets, Secular evolution of compact binaries near massive black holes: Gravitational wave sources and other exotica, *Astrophys. J.* **757**, 27 (2012), [arXiv:1203.2938](#) [astro-ph.GA].

[59] J. M. Antognini, B. J. Shappee, T. A. Thompson,

and P. Amaro-Seoane, Rapid Eccentricity Oscillations and the Mergers of Compact Objects in Hierarchical Triples, *Mon. Not. Roy. Astron. Soc.* **439**, 1079 (2014), arXiv:1308.5682 [astro-ph.HE].

[60] J. H. VanLandingham, M. C. Miller, D. P. Hamilton, and D. C. Richardson, The Role of the Kozai–lidakov Mechanism in Black Hole Binary Mergers in Galactic Centers, *Astrophys. J.* **828**, 77 (2016), arXiv:1604.04948 [astro-ph.HE].

[61] F. Antonini, S. Toonen, and A. S. Hamers, Binary black hole mergers from field triples: properties, rates and the impact of stellar evolution, *Astrophys. J.* **841**, 77 (2017), arXiv:1703.06614 [astro-ph.GA].

[62] M. Zevin, I. M. Romero-Shaw, K. Kremer, E. Thrane, and P. D. Lasky, Implications of Eccentric Observations on Binary Black Hole Formation Channels, *Astrophys. J. Lett.* **921**, L43 (2021), arXiv:2106.09042 [astro-ph.HE].

[63] B. Sun, Z. Cao, Y. Wang, and H.-C. Yeh, Parameter estimation of eccentric inspiraling compact binaries using an enhanced post circular model for ground-based detectors, *Phys. Rev. D* **92**, 044034 (2015).

[64] S. Ma, Z. Cao, C.-Y. Lin, H.-P. Pan, and H.-J. Yo, Gravitational wave source localization for eccentric binary coalesce with a ground-based detector network, *Phys. Rev. D* **96**, 084046 (2017), arXiv:1710.02965 [gr-qc].

[65] H.-P. Pan, C.-Y. Lin, Z. Cao, and H.-J. Yo, Accuracy of source localization for eccentric inspiraling binary mergers using a ground-based detector network, *Phys. Rev. D* **100**, 124003 (2019), arXiv:1912.04455 [gr-qc].

[66] T. Yang, R.-G. Cai, Z. Cao, and H. M. Lee, Eccentricity of Long Inspiraling Compact Binaries Sheds Light on Dark Sirens, *Phys. Rev. Lett.* **129**, 191102 (2022), arXiv:2202.08608 [gr-qc].

[67] T. Yang, R.-G. Cai, and H. M. Lee, Space-borne atom interferometric gravitational wave detections. Part III. Eccentricity on dark sirens, *JCAP* **10**, 061, arXiv:2208.10998 [gr-qc].

[68] T. Yang, R.-G. Cai, Z. Cao, and H. M. Lee, Parameter estimation of eccentric gravitational waves with a decihertz observatory and its cosmological implications, *Phys. Rev. D* **107**, 043539 (2023), arXiv:2212.11131 [gr-qc].

[69] T. Yang, R.-G. Cai, Z. Cao, and H. M. Lee, Eccentricity enables the earliest warning and localization of gravitational waves with ground-based detectors, *Phys. Rev. D* **109**, 104041 (2024), arXiv:2310.08160 [gr-qc].

[70] T. Yang, R.-G. Cai, Z. Cao, and H. M. Lee, The Advantage of Early Detection and Localization from Eccentricity-Induced Higher Harmonic Modes in Second-Generation Ground-Based Detector Networks (2024), arXiv:2412.20664 [gr-qc].

[71] M. Favata, Systematic parameter errors in inspiraling neutron star binaries, *Phys. Rev. Lett.* **112**, 101101 (2014), arXiv:1310.8288 [gr-qc].

[72] H. Gil Choi, T. Yang, and H. M. Lee, Importance of eccentricities in parameter estimation of compact binary inspirals with decihertz gravitational-wave detectors, *Phys. Rev. D* **110**, 024025 (2024), arXiv:2210.09541 [gr-qc].

[73] P. Saini, M. Favata, and K. G. Arun, Systematic bias on parametrized tests of general relativity due to neglect of orbital eccentricity, *Phys. Rev. D* **106**, 084031 (2022), arXiv:2203.04634 [gr-qc].

[74] P. Narayan, N. K. Johnson-McDaniel, and A. Gupta, Effect of ignoring eccentricity in testing general relativity with gravitational waves, *Phys. Rev. D* **108**, 064003 (2023), arXiv:2306.04068 [gr-qc].

[75] Divyajyoti, S. Kumar, S. Tibrewal, I. M. Romero-Shaw, and C. K. Mishra, Blind spots and biases: The dangers of ignoring eccentricity in gravitational-wave signals from binary black holes, *Phys. Rev. D* **109**, 043037 (2024), arXiv:2309.16638 [gr-qc].

[76] B. Gadre, K. Soni, S. Tiwari, A. Ramos-Buades, M. Haney, and S. Mitra, Detectability of eccentric binary black holes with matched filtering and unmodeled pipelines during the third observing run of LIGO–Virgo–KAGRA, *Phys. Rev. D* **110**, 044013 (2024), arXiv:2405.04186 [gr-qc].

[77] J.-Z. Yang, J.-H. Zhong, and T. Yang, Systematic Biases in Gravitational-Wave Parameter Estimation from Neglecting Orbital Eccentricity in Space-Based Detectors (2026), arXiv:2601.07739 [gr-qc].

[78] B. P. Abbott *et al.* (LIGO Scientific, Virgo), Search for Eccentric Binary Black Hole Mergers with Advanced LIGO and Advanced Virgo during their First and Second Observing Runs, *Astrophys. J.* **883**, 149 (2019), arXiv:1907.09384 [astro-ph.HE].

[79] A. G. Abac *et al.* (LIGO Scientific, KAGRA, VIRGO), Search for Eccentric Black Hole Coalescences during the Third Observing Run of LIGO and Virgo, *Astrophys. J.* **973**, 132 (2024), arXiv:2308.03822 [astro-ph.HE].

[80] I. M. Romero-Shaw, P. D. Lasky, E. Thrane, and J. C. Bustillo, GW190521: orbital eccentricity and signatures of dynamical formation in a binary black hole merger signal, *Astrophys. J. Lett.* **903**, L5 (2020), arXiv:2009.04771 [astro-ph.HE].

[81] I. M. Romero-Shaw, P. D. Lasky, and E. Thrane, Signs of Eccentricity in Two Gravitational-wave Signals May Indicate a Subpopulation of Dynamically Assembled Binary Black Holes, *Astrophys. J. Lett.* **921**, L31 (2021), arXiv:2108.01284 [astro-ph.HE].

[82] I. M. Romero-Shaw, P. D. Lasky, and E. Thrane, Four Eccentric Mergers Increase the Evidence that LIGO–Virgo–KAGRA’s Binary Black Holes Form Dynamically, *Astrophys. J.* **940**, 171 (2022), arXiv:2206.14695 [astro-ph.HE].

[83] V. Gayathri, J. Healy, J. Lange, B. O’Brien, M. Szczepanczyk, I. Bartos, M. Campanelli, S. Klimenko, C. O. Lousto, and R. O’Shaughnessy, Eccentricity estimate for black hole mergers with numerical relativity simulations, *Nature Astron.* **6**, 344 (2022), arXiv:2009.05461 [astro-ph.HE].

[84] N. Gupte, A. Ramos-Buades, A. Buonanno, J. Gair, M. C. Miller, M. Dax, S. R. Green, M. Pürer, J. Wildberger, J. Macke, I. M. Romero-Shaw, and B. Schölkopf, Evidence for eccentricity in the population of binary black holes observed by ligo-virgo-kagra (2024), arXiv:2404.14286 [gr-qc].

[85] M. de Lluc Planas, A. Ramos-Buades, C. García-Quirós, H. Estellés, S. Husa, and M. Haney, Eccentric or circular? a reanalysis of binary black hole gravitational wave events for orbital eccentricity signatures (2025), arXiv:2504.15833 [gr-qc].

[86] R. Abbott *et al.* (LIGO Scientific, Virgo), Properties and Astrophysical Implications of the $150 M_{\odot}$ Binary Black Hole Merger GW190521, *Astrophys. J. Lett.* **900**, L13 (2020), arXiv:2009.01190 [astro-ph.HE].

[87] M. J. Graham *et al.*, Candidate Electromagnetic Counterpart to the Binary Black Hole Merger Gravitational Wave Event S190521g, *Phys. Rev. Lett.* **124**, 251102 (2020), arXiv:2006.14122 [astro-ph.HE].

[88] H. L. Iglesias *et al.*, Eccentricity Estimation for Five Binary Black Hole Mergers with Higher-order Gravitational-wave Modes, *Astrophys. J.* **972**, 65 (2024), arXiv:2208.01766 [gr-qc].

[89] A. Ramos-Buades, A. Buonanno, and J. Gair, Bayesian inference of binary black holes with inspiral-merger-ringdown waveforms using two eccentric parameters, *Phys. Rev. D* **108**, 124063 (2023), arXiv:2309.15528 [gr-qc].

[90] A. Gamboa *et al.*, Accurate waveforms for eccentric, aligned-spin binary black holes: The multipolar effective-one-body model seobnrv5ehm, *Phys. Rev. D* **112**, 044038 (2025), arXiv:2412.12823 [gr-qc].

[91] V. Varma, P. Ajith, S. Husa, J. C. Bustillo, M. Hannam, and M. Pürller, Gravitational-wave observations of binary black holes: Effect of nonquadrupole modes, *Phys. Rev. D* **90**, 124004 (2014), arXiv:1409.2349 [gr-qc].

[92] R. S. Chandramouli, K. Prokup, E. Berti, and N. Yunes, Systematic biases due to waveform mismodeling in parametrized post-Einsteinian tests of general relativity: The impact of neglecting spin precession and higher modes, *Phys. Rev. D* **111**, 044026 (2025), arXiv:2410.06254 [gr-qc].

[93] S. Yi, F. Iacovelli, S. Marsat, D. Wadekar, and E. Berti, Systematic biases from the exclusion of higher harmonics in parameter estimation on lisa binaries (2025), arXiv:2502.12237 [gr-qc].

[94] N. Yunes, K. G. Arun, E. Berti, and C. M. Will, Post-Circular Expansion of Eccentric Binary Inspirals: Fourier-Domain Waveforms in the Stationary Phase Approximation, *Phys. Rev. D* **80**, 084001 (2009), [Erratum: Phys. Rev. D 89, 109901 (2014)], arXiv:0906.0313 [gr-qc].

[95] N. J. Cornish and J. Shapiro Key, Computing waveforms for spinning compact binaries in quasi-eccentric orbits, *Phys. Rev. D* **82**, 044028 (2010), [Erratum: Phys. Rev. D 84, 029901 (2011)], arXiv:1004.5322 [gr-qc].

[96] J. Shapiro Key and N. J. Cornish, Characterizing Spinning Black Hole Binaries in Eccentric Orbits with LISA, *Phys. Rev. D* **83**, 083001 (2011), arXiv:1006.3759 [gr-qc].

[97] E. A. Huerta, P. Kumar, S. T. McWilliams, R. O’Shaughnessy, and N. Yunes, Accurate and efficient waveforms for compact binaries on eccentric orbits, *Phys. Rev. D* **90**, 084016 (2014), arXiv:1408.3406 [gr-qc].

[98] N. Loutrel and N. Yunes, Eccentric Gravitational Wave Bursts in the Post-Newtonian Formalism, *Class. Quant. Grav.* **34**, 135011 (2017), arXiv:1702.01818 [gr-qc].

[99] S. Tanay, M. Haney, and A. Gopakumar, Frequency and time domain inspiral templates for comparable mass compact binaries in eccentric orbits, *Phys. Rev. D* **93**, 064031 (2016), arXiv:1602.03081 [gr-qc].

[100] B. Moore, M. Favata, K. G. Arun, and C. K. Mishra, Gravitational-wave phasing for low-eccentricity inspiralling compact binaries to 3PN order, *Phys. Rev. D* **93**, 124061 (2016), arXiv:1605.00304 [gr-qc].

[101] B. Moore, T. Robson, N. Loutrel, and N. Yunes, Towards a Fourier domain waveform for non-spinning binaries with arbitrary eccentricity, *Class. Quant. Grav.* **35**, 235006 (2018), arXiv:1807.07163 [gr-qc].

[102] B. Moore and N. Yunes, A 3PN Fourier Domain Waveform for Non-Spinning Binaries with Moderate Eccentricity, *Class. Quant. Grav.* **36**, 185003 (2019), arXiv:1903.05203 [gr-qc].

[103] A. Klein, Y. Boetzel, A. Gopakumar, P. Jetzer, and L. de Vittori, Fourier domain gravitational waveforms for precessing eccentric binaries, *Phys. Rev. D* **98**, 104043 (2018), arXiv:1801.08542 [gr-qc].

[104] A. Klein, Efpe: Efficient fully precessing eccentric gravitational waveforms for binaries with long inspirals (2021), arXiv:2106.10291 [gr-qc].

[105] E. A. Huerta *et al.*, Complete waveform model for compact binaries on eccentric orbits, *Phys. Rev. D* **95**, 024038 (2017), arXiv:1609.05933 [gr-qc].

[106] E. A. Huerta *et al.*, Eccentric, nonspinning, inspiral, Gaussian-process merger approximant for the detection and characterization of eccentric binary black hole mergers, *Phys. Rev. D* **97**, 024031 (2018), arXiv:1711.06276 [gr-qc].

[107] I. Hinder, L. E. Kidder, and H. P. Pfeiffer, Eccentric binary black hole inspiral-merger-ringdown gravitational waveform model from numerical relativity and post-Newtonian theory, *Phys. Rev. D* **98**, 044015 (2018), arXiv:1709.02007 [gr-qc].

[108] A. Ramos-Buades, S. Husa, G. Pratten, H. Estellés, C. García-Quirós, M. Mateu-Lucena, M. Colleoni, and R. Jaume, First survey of spinning eccentric black hole mergers: Numerical relativity simulations, hybrid waveforms, and parameter estimation, *Phys. Rev. D* **101**, 083015 (2020), arXiv:1909.11011 [gr-qc].

[109] A. Chattaraj, T. RoyChowdhury, Divyajyoti, C. K. Mishra, and A. Gupta, High accuracy post-Newtonian and numerical relativity comparisons involving higher modes for eccentric binary black holes and a dominant mode eccentric inspiral-merger-ringdown model, *Phys. Rev. D* **106**, 124008 (2022), arXiv:2204.02377 [gr-qc].

[110] P. Manna, T. RoyChowdhury, and C. K. Mishra, Improved inspiral-merger-ringdown model for BBHs on elliptical orbits, *Phys. Rev. D* **111**, 124026 (2025), arXiv:2409.10672 [gr-qc].

[111] K. Paul, A. Maurya, Q. Henry, K. Sharma, P. Satheesh, Divyajyoti, P. Kumar, and C. K. Mishra, Eccentric, spinning, inspiral-merger-ringdown waveform model with higher modes for the detection and characterization of binary black holes, *Phys. Rev. D* **111**, 084074 (2025), arXiv:2409.13866 [gr-qc].

[112] T. Islam, V. Varma, J. Lodman, S. E. Field, G. Khanna, M. A. Scheel, H. P. Pfeiffer, D. Gerosa, and L. E. Kidder, Eccentric binary black hole surrogate models for the gravitational waveform and remnant properties: comparable mass, nonspinning case, *Phys. Rev. D* **103**, 064022 (2021), arXiv:2101.11798 [gr-qc].

[113] Z. Cao and W.-B. Han, Waveform model for an eccentric binary black hole based on the effective-one-body-numerical-relativity formalism, *Phys. Rev. D* **96**, 044028 (2017), arXiv:1708.00166 [gr-qc].

[114] X. Liu, Z. Cao, and L. Shao, Validating the Effective-One-Body Numerical-Relativity Waveform Models for Spin-aligned Binary Black Holes along Eccentric Orbits, *Phys. Rev. D* **101**, 044049 (2020), arXiv:1910.00784 [gr-qc].

[115] X. Liu, Z. Cao, and Z.-H. Zhu, A higher-multipole gravitational waveform model for an eccentric binary

black holes based on the effective-one-body-numerical-relativity formalism, *Class. Quant. Grav.* **39**, 035009 (2022), arXiv:2102.08614 [gr-qc].

[116] A. Ramos-Buades, A. Buonanno, M. Khalil, and S. Ossokine, Effective-one-body multipolar waveforms for eccentric binary black holes with nonprecessing spins, *Phys. Rev. D* **105**, 044035 (2022), arXiv:2112.06952 [gr-qc].

[117] A. Nagar, A. Bonino, and P. Rettegno, Effective one-body multipolar waveform model for spin-aligned, quasicircular, eccentric, hyperbolic black hole binaries, *Phys. Rev. D* **103**, 104021 (2021), arXiv:2101.08624 [gr-qc].

[118] A. Nagar, R. Gamba, P. Rettegno, V. Fantini, and S. Bernuzzi, Effective-one-body waveform model for noncircularized, planar, coalescing black hole binaries: The importance of radiation reaction, *Phys. Rev. D* **110**, 084001 (2024), arXiv:2404.05288 [gr-qc].

[119] M. de Lluc Planas, A. Ramos-Buades, C. García-Quirós, H. Estellés, S. Husa, and M. Haney, Time-domain phenomenological multipolar waveforms for aligned-spin binary black holes in elliptical orbits (2025), arXiv:2503.13062 [gr-qc].

[120] X. Liu, Z. Cao, and Z.-H. Zhu, Effective-one-body numerical-relativity waveform model for eccentric spin-precessing binary black hole coalescence, *Class. Quant. Grav.* **41**, 195019 (2024), arXiv:2310.04552 [gr-qc].

[121] D. P. Mihaylov, S. Ossokine, A. Buonanno, H. Estelles, L. Pompili, M. Pürrer, and A. Ramos-Buades, pySEOBNR: a software package for the next generation of effective-one-body multipolar waveform models, *SoftwareX* **30**, 102080 (2025), arXiv:2303.18203 [gr-qc].

[122] L. Pompili *et al.*, Laying the foundation of the effective-one-body waveform models SEOBNRv5: Improved accuracy and efficiency for spinning nonprecessing binary black holes, *Phys. Rev. D* **108**, 124035 (2023), arXiv:2303.18039 [gr-qc].

[123] E. Thrane and C. Talbot, An introduction to Bayesian inference in gravitational-wave astronomy: parameter estimation, model selection, and hierarchical models, *Publ. Astron. Soc. Austral.* **36**, e010 (2019), [Erratum: *Publ. Astron. Soc. Austral.* 37, e036 (2020)], arXiv:1809.02293 [astro-ph.IM].

[124] I. M. Romero-Shaw *et al.*, Bayesian inference for compact binary coalescences with bilby: validation and application to the first LIGO–Virgo gravitational-wave transient catalogue, *Mon. Not. Roy. Astron. Soc.* **499**, 3295 (2020), arXiv:2006.00714 [astro-ph.IM].

[125] G. Ashton *et al.*, BILBY: A user-friendly Bayesian inference library for gravitational-wave astronomy, *Astrophys. J. Suppl.* **241**, 27 (2019), arXiv:1811.02042 [astro-ph.IM].

[126] J. S. Speagle, dynesty: a dynamic nested sampling package for estimating Bayesian posteriors and evidences, *Mon. Not. Roy. Astron. Soc.* **493**, 3132 (2020), arXiv:1904.02180 [astro-ph.IM].

[127] J. Lin, Divergence measures based on the Shannon entropy, *IEEE Trans. Info. Theor.* **37**, 145 (1991).

[128] P. Virtanen, R. Gommers, T. E. Oliphant, M. Haberland, T. Reddy, D. Cournapeau, E. Burovski, P. Peterson, W. Weckesser, J. Bright, S. J. van der Walt, M. Brett, J. Wilson, K. J. Millman, N. Mayorov, A. R. J. Nelson, E. Jones, R. Kern, E. Larson, C. J. Carey, İ. Polat, Y. Feng, E. W. Moore, J. VanderPlas, D. Laxalde, J. Perktold, R. Cimrman, I. Henriksen, E. A. Quintero, C. R. Harris, A. M. Archibald, A. H. Ribeiro, F. Pedregosa, P. van Mulbregt, and SciPy 1.0 Contributors, SciPy 1.0: Fundamental Algorithms for Scientific Computing in Python, *Nature Methods* **17**, 261 (2020).

[129] R. Abbott *et al.* (KAGRA, VIRGO, LIGO Scientific), Open Data from the Third Observing Run of LIGO, Virgo, KAGRA, and GEO, *Astrophys. J. Suppl.* **267**, 29 (2023), arXiv:2302.03676 [gr-qc].

[130] L. S. Collaboration and V. Collaboration, Gwtc-2.1: Deep extended catalog of compact binary coalescences observed by ligo and virgo during the first half of the third observing run – glitch modelling for events, 10.5281/zenodo.6477076 (2022).

[131] L. S. Collaboration, V. Collaboration, and K. Collaboration, Gwtc-3: Compact binary coalescences observed by ligo and virgo during the second part of the third observing run — glitch modelling for events, 10.5281/zenodo.5546680 (2021).

[132] N. J. Cornish and T. B. Littenberg, BayesWave: Bayesian Inference for Gravitational Wave Bursts and Instrument Glitches, *Class. Quant. Grav.* **32**, 135012 (2015), arXiv:1410.3835 [gr-qc].

[133] D. Davis, T. J. Massinger, A. P. Lundgren, J. C. Driggers, A. L. Urban, and L. K. Nuttall, Improving the Sensitivity of Advanced LIGO Using Noise Subtraction, *Class. Quant. Grav.* **36**, 055011 (2019), arXiv:1809.05348 [astro-ph.IM].

[134] D. Davis, T. B. Littenberg, I. M. Romero-Shaw, M. Millhouse, J. McIver, F. Di Renzo, and G. Ashton, Subtracting glitches from gravitational-wave detector data during the third LIGO-Virgo observing run, *Class. Quant. Grav.* **39**, 245013 (2022), arXiv:2207.03429 [astro-ph.IM].

[135] L. Pekowsky, J. Healy, D. Shoemaker, and P. Laguna, Impact of higher-order modes on the detection of binary black hole coalescences, *Phys. Rev. D* **87**, 084008 (2013), arXiv:1210.1891 [gr-qc].

[136] C. Cutler and M. Vallisneri, LISA detections of massive black hole inspirals: Parameter extraction errors due to inaccurate template waveforms, *Phys. Rev. D* **76**, 104018 (2007), arXiv:0707.2982 [gr-qc].

[137] V. De Luca, L. Del Grosso, F. Iacovelli, A. Maselli, and E. Berti, Systematic biases from ignoring environmental tidal effects in gravitational wave observations, *Phys. Rev. D* **111**, 124046 (2025), arXiv:2503.10746 [gr-qc].

[138] C. Hoy and V. Raymond, PESummary: the code agnostic Parameter Estimation Summary page builder, *SoftwareX* **15**, 100765 (2021), arXiv:2006.06639 [astro-ph.IM].